

# Microwave-assisted synthesis of graphene nanocomposites: recent developments on lithium-ion batteries

Weiwei Sun

Hao Li

Yong Wang

Department of Chemical Engineering,  
School of Environmental and  
Chemical Engineering, Shanghai  
University, Shanghai, People's  
Republic of China

**Abstract:** Lithium ion battery (LIB) is a popular power source for various portable mobile devices and even electrical vehicles. Graphene-based composites are important electrodes for LIBs due to their high-capacity, long cycle life, and impressive high-rate capability. Microwave-assisted synthesis is a promising approach to prepare graphene-based composites owing to its fast, energy-efficient features. By varying microwave irradiation conditions, surface functionality and morphology control can be tuned for either graphene or the introduced secondary phase in the graphene-based composites. When used for LIBs, the graphene-based composites can offer a variety of merits for the improved electrochemical properties such as facilitated lithium diffusion/storage and the increased mechanical stability of the electrodes during repetitive cycling. This article reviews the recent progress of microwave-assisted synthesis of graphene-based electrodes and their applications for LIBs. Graphene-supported transitional metal oxides anodes (Li-storage conversion mechanism), tin/germanium/silicon based anodes (lithium alloy mechanism), metal sulfides (conversion or lithium alloy mechanism), lithium-titanium-oxide-based anodes (lithium insertion mechanism), and graphene-decorated lithium iron phosphate cathodes are reviewed with more emphasis because these materials have attracted significant research concerns. The effect of microwave irradiation and the resultant structure and size control of graphene-based composites on their electrochemical properties is also elucidated.

**Keywords:** electrode, graphene, lithium ion batteries, microwave irradiation, nanocomposites

## Introduction

With the development of electrical energy-storage materials to meet the increasing demand for the ever-growing energy consumption, lithium-ion battery (LIB), with excellence in terms of high energy density, no memory effect, long cycle life, and environmental friendliness, has been an attractive power source for portable mobile devices and stationary energy storage.<sup>1-4</sup> As the commercial anode for LIBs, graphite gradually cannot satisfy the requirements of the ever-growing advanced high-power LIBs and new anode materials with higher energy density and power density must be explored.<sup>5-8</sup> Since the discovery in 2004, graphene has attracted significant research concerns for various energy-related applications including LIBs,<sup>9-11</sup> solar cells,<sup>12-14</sup> supercapacitors,<sup>15-17</sup> and fuel cells.<sup>18-21</sup> This is largely ascribed to its intriguing properties associated with the unique single-atom layered structure such as a large theoretical specific surface area of 2,600 m<sup>2</sup> g<sup>-1</sup>,<sup>22</sup> highly flexible but robust mechanical structure, and fast electronic conduction. As an anode for LIBs, graphene was reported with a reversible capacity of ~400–1,100 mAh g<sup>-1</sup>,<sup>23-26</sup> and its unsatisfactory cyclability has been mainly ascribed to its heavy agglomeration during cycling,

Correspondence: Yong Wang  
Department of Chemical Engineering,  
School of Environmental and Chemical  
Engineering, Shanghai University,  
Shangda Road 99, Shanghai 200444,  
People's Republic of China  
Tel +86 21 6613 7723  
Fax +86 21 6613 7725  
Email yongwang@shu.edu.cn

which leads to the loss of promising properties relative to the atomic-thickness structure. An effective strategy is to introduce the secondary phase to the graphene, which acts as a spacer to separate few-layer graphene nanosheets (GNS) and prevent their restacking to graphite platelets.<sup>27–29</sup> The introduced component is usually also highly active for lithium-ion storage, and therefore, there is no capacity loss for the resultant composites. Moreover, the presence of graphene is also very beneficial for the improvement of the electrical conductivity and mechanical stability to the introduced secondary phase. As a result, graphene-supported composites can exhibit synergetic effect with respect to lithium-ion storage properties and achieve better electrochemical performance, especially long cycle life and impressive high-rate capability.<sup>30</sup>

GNS used for fabrication of lithium ion anode materials were mostly synthesized through the chemical oxidation and reduction approach. The exfoliation and reduction of graphene oxide (GO) is the most important step to obtain GNS with suitable functionalities and reduction extents, which strongly affect the electrochemical properties of graphene or graphene-based composite electrodes. However, the exfoliation and reduction of GO rely heavily on the usage of strong reducing agents or a very high temperature. Most of these approaches are complicated, energy, and cost intensive. Recently, microwave exfoliation has been proved to be an attractive method for graphene preparation<sup>31–33</sup> because it is a facile, time-efficient, and cost-effective process. Besides, the obtained graphene via microwave-assisted methods can exhibit larger average size, higher quality with residual functional groups, and better electrochemical properties for LIBs compared with those prepared from conventional methods.<sup>34–36</sup>

Microwaves have been widely used in industrial applications such as food processing<sup>37,38</sup> and industrial materials.<sup>39,40</sup> Motivated by its advantages of facile, fast, secure, controllable, and energy-saving characteristics, microwave-assisted technique has achieved rapid development in the field of materials science.<sup>41,42</sup> Microwave-assisted techniques such as solid-state microwave irradiation, microwave-assisted solvothermal/hydrothermal process can provide simple and fast routes to synthesize nanomaterials without high temperature or high pressure. Furthermore, the microwave technique is particularly useful for a large-scale synthesis without complicated preparation conditions.<sup>43–46</sup> The rapid transfer of energy and fast decomposition of the precursors provided by microwave source would result in highly effective local reaction temperatures and significant enhancement in reaction rates.

Besides, the microwave technique can provide an effective way to control particle size distribution and macroscopic morphology during the synthesis process because it can heat a substance uniformly and therefore a more homogeneous nucleation environment and a shorter crystallization time can be achieved compared to conventional heating.

In this review, we aim to investigate the mechanism of microwave-assisted syntheses of graphene and graphene-based nanocomposites, and summarize the recent development of graphene-supported nanocomposites for applications as electrodes for LIBs. Various types of graphene-based nanomaterials: mainly graphene-based transitional metal oxide anodes, tin/germanium/silicon based anodes, metal sulfides anodes, lithium-titanium-oxide-based anodes and graphene-decorated lithium iron phosphate cathodes are presented and discussed with respect to their morphological and size control in the microwave-assisted preparation process and their relation to the resultant lithium storage properties.

## Mechanism of microwave-assisted syntheses

Microwave irradiation is an electromagnetic irradiation in the range of wavelengths from 0.01 m to 1 m with corresponding frequency range from 300 MHz to 300 GHz.<sup>47</sup> The domestic microwave generally owns a frequency of 2.45 GHz (a wavelength of 12.25 cm), while the industrial microwave usually owns two frequencies of 915 MHz and 2.45 GHz.<sup>37</sup> Microwave has been widely used for heating those materials, which can absorb microwave energy and convert it into heat. In the presence of moisture or water, dielectric heating happens due to the dipolar nature of water. These permanently polarized dipolar molecules could rearrange in the direction of the electric field at a high speed, which would cause internal friction of molecules and further result in the volumetric heating of the whole material. Besides the dipolar mechanism, microwave heating may also occur due to the ionic mechanism, and oscillatory migration of ions in the material would generate heat under a high-frequency oscillating electric field.<sup>48</sup> Consequently, microwave-assisted technology can provide a fast and effective approach to heat the material/system homogeneously from the interior. In contrast, traditional heating system, in which heat is transferred from the surface toward the center of the material under the help of heating mantle, water/oil bath or other external heat source, is relatively slow and inefficient.

GNS are usually obtained from graphite or GO, which is prepared by a modified Hummer's method.<sup>49–51</sup> The reduction of GO is usually carried out by chemical methods in the

presence of various hazardous reduction agents such as hydrazine and  $\text{NaBH}_4$ . In comparison, thermal treatment is a green method because no hazardous reduction agents are used. Instead of the conventional preparation of graphene in traditional heating system (furnace or oil bath), the eco-friendly microwave-assisted method has attracted increasing attentions in which the microwave-assisted solvothermal/hydrothermal methods can be adopted to treat GO<sup>52,53</sup> or natural graphite<sup>54–57</sup> in a microwave oven or microwave plasma-enhanced chemical vapor deposition (MPCVD) system.<sup>58–60</sup> It is worth noting that the microwave exfoliation is an attractive and effective method for graphene synthesis from GO, in which GO is exfoliated with nontoxic solvents within a short reaction time of 1–15 minutes at a relatively low temperature range of 180°C–300°C.<sup>52,53</sup> It was reported that the stable graphene suspension could be obtained from the GO suspension in an alkaline medium ( $\text{pH} \approx 10$ ) or polar solvents (*N,N*-dimethylformamide, ethanol, 1-butanol, and water) in a facile microwave-assisted solvothermal process.<sup>61,62</sup> Besides, the water-soluble polymer-grafted graphene sheets were prepared from GO in a household microwave oven at a power of 450 W for 4 minutes.<sup>63</sup> The synthesis of three-dimensional (3D) nanostructure of “graphene nano-cup” anchored on the few layered graphene substrate<sup>64</sup> under the microwave irradiation in a domestic microwave oven was reported by two steps: one-pot synthesis of graphene-coated metal nanoparticles anchored on the graphene sheets and the subsequent etching of metals. Furthermore, giant graphene sheets could be obtained by double microwave-assisted exfoliation of expandable graphite<sup>65</sup> and highly hydrogenated graphene could be produced from GO by a one-step microwave irradiation process in hydrogen plasma, in which the deoxidation and concurrent hydrogenation were both achieved.<sup>66</sup> A possible mechanism of graphene preparation by a microwave-assisted technology is illuminated in Figure 1. The microwave irradiation provides high local temperature and pressure atmosphere, and energy is transferred directly into the GO interior. Heat is produced from the interaction of irradiation with the polar bond of oxygen-containing

functional groups on the surface and edge of GO sheets. Besides, the interaction between polar solvent and surface oxides on GO sheets is an important factor to determine the uniformity of deposits. Furthermore, the functional groups on the surface of GO are effectively reduced, and the reduction degree of graphene sheets is further improved.

The microwave-assisted technology for the synthesis of graphene has several obvious advantages. First, the microwave-assisted process is time-efficient without complicated synthesis procedure. Second, such process is cost-effective as the quantity of the used chemicals is greatly reduced compared to conventional approaches. Third, the average size of the obtained graphene from microwave-assisted technology can be ten times larger than those prepared by the conventional heating method. Finally, the graphene products from microwave-assisted technology are of high quality with controlled structure and residual functional groups.

Until now, microwave irradiation has been suggested as an effective tool to obtain carbon-relative composites with uniform dispersion and size and morphology control,<sup>67–69</sup> because the microwave energy allows rapid heating and extremely rapid rate of crystallization to produce the desired nanocrystalline products. Meanwhile, during the microwave-assisted synthesis process, it is possible to control the growth of the favorable crystallographic plane by varying reaction time and the relative concentrations of different organic surfactants. Furthermore, the obtained nanostructures would extend from small spherical nuclei to short nanorod or nanosheet.<sup>70–72</sup> As a result, various graphene-based nanocomposites with controlled size and shape, such as particle/crystal-on-sheet, nanorod/nanofiber-on-sheet, and nanosheet-on-sheet, can be obtained with the help of ecofriendly microwave-assisted technology, as illuminated in Figure 1. It is worthy noting that the hydrothermal/solvothermal processes operated in a single-mode microwave reaction or a multimode household microwave oven are the most used technology for the microwave-assisted synthesis of graphene-based nanocomposites. Nonuniform microwave is offered from multimode domestic microwave oven, in which

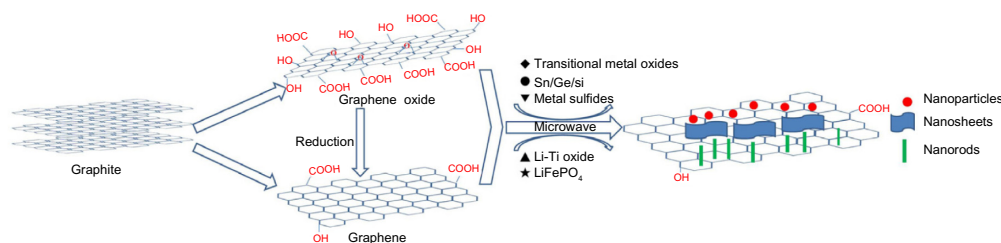


**Figure 1** Schematic illustration of the synthesis of graphene and graphene-based composites with the assistance of microwave irradiation.

there is considerable variation in the microwave intensity throughout the reactor chamber. Moreover, the multimode domestic microwave oven can only roughly provide the time and several stages of power control (such as high, medium, low). In comparison, very uniform microwave can be generated in the specialized single-mode microwave reactor with stable microwave intensity in the chamber in which power, temperature, and time can be fine-tuned with continuous magnetic stirring. Therefore, the reaction environment is more uniform in the single-mode microwave reactor and better size and shape control should be achieved.

## GNS-supported transitional metal oxide anodes

The microwave irradiation method has been applied for the synthesis of GNS-supported transitional metal oxide electrodes such as  $\text{Co}_3\text{O}_4$ -GNS,<sup>73–77</sup>  $\text{CuO}$ -GNS,<sup>78–83</sup> and  $\text{Fe}_x\text{O}_y$ -GNS.<sup>84–89</sup> All these transitional metal oxides have approximately two to three times larger theoretical capacities than commercial graphite anode based on a well-known conversion mechanism of lithium storage. Lithium can reduce metal oxides to metal and form lithium oxide, and this reaction is reversible. The morphologies and lithium-storage properties of various graphene-supported transitional metal oxide anodes are summarized in Table 1. Among these GNS-supported transitional metal oxide anodes,  $\text{Co}_3\text{O}_4$ -GNS tends to form a particle-on-nanosheet morphology under microwave irradiation.<sup>73–76</sup> As reported by Wang et al,<sup>77</sup> two-dimensional (2D) porous  $\text{Co}_3\text{O}_4$  nanosheets were obtained by a microwave solvothermal process at 180°C for 5 minutes (pressure: ~7.5 bar) in a single-mode microwave reactor (Nova, EU Microwave Chemistry, Shanghai, People's Republic of China). As shown in Figure 2, these porous  $\text{Co}_3\text{O}_4$  nanosheets have pore sizes of 60–100 nm and a thickness around 100 nm. After stacking with graphene, the  $\text{Co}_3\text{O}_4$ -GNS composite can form a sheet-on-sheet composite structure.<sup>77</sup> The sheet-on-sheet composite shows superior Li-ion storage performances. Initial reversible charge capacity of 1,235  $\text{mAh g}^{-1}$  is delivered, which decreases to 1,065  $\text{mAh g}^{-1}$  after 30 cycles. This capacity is larger than those of GO or GNS, and even the theoretical value of pristine  $\text{Co}_3\text{O}_4$  (890  $\text{mAh g}^{-1}$ ). The composite also exhibits an impressive good high-rate capability (a reversible capacity of 931  $\text{mAh g}^{-1}$  at a large current rate of 5 C [4,450  $\text{mA g}^{-1}$ , 5 C represents the current at which the cell capacity is charged/discharged in 1/5 h]).

Synthesized by the microwave-assisted technology, GNS-supported copper oxides can exhibit a variety of morphologies including zero-dimensional (0D) nanoparticle<sup>78/</sup>

nanosphere,<sup>79,80</sup> one-dimensional (1D) nanowire<sup>81</sup>/fusiform,<sup>82</sup> and 2D nanoleaf<sup>83</sup>/nanosheet<sup>82</sup> morphologies. Among them, GNS-supported copper oxides with higher dimensional (1D and 2D)<sup>81–83</sup> or core-shell morphology<sup>79</sup> exhibit better electrochemical performance. By a fast single-mode microwave hydrothermal method, the GNS-supported sheet-like or fusiform-like  $\text{CuO}$  morphologies were obtained by varying the reaction temperature of microwave heating. As shown in Figure 3A–C,<sup>82</sup>  $\text{CuO}$ -GNS sheet-on-sheet product was prepared at 170°C with  $\text{CuO}$  nanosheet of 0.3–0.5  $\mu\text{m}$  in size, while the  $\text{CuO}$ -GNS fusiform-on-sheet material was obtained at a lower temperature of 110°C with fusiform  $\text{CuO}$  product owning the length around 0.4–0.8  $\mu\text{m}$  and narrow tips. Figure 3D shows the electrochemical performance of the above two  $\text{CuO}$ -GNS composites in comparison with the physical mixture of  $\text{CuO}$  and GNS. Reversible charge capacities of 801 and 666  $\text{mAh g}^{-1}$  can be retained after 40 cycles for graphene-supported  $\text{CuO}$  nanosheet and fusiform composites, respectively. These reversible capacities are substantially larger than that of  $\text{CuO}$ -GNS (431  $\text{mAh g}^{-1}$ ) by a physical mixture after the same cycle numbers. As shown in Figure 3E, the graphene-supported  $\text{CuO}$  nanosheet composite exhibits an excellent rate capability with initial charge capacities of 981, 925, and 846  $\text{mAh g}^{-1}$  at 1, 2, and 5 C, respectively (1 C = 700  $\text{mA g}^{-1}$ ).

The  $\text{Fe}_2\text{O}_3$ -GNS composite with porous nanorod-on-sheet morphology was synthesized by a solvothermal process in a microwave oven.<sup>84</sup> The composite delivers a high reversible initial capacity of 1,016  $\text{mAh g}^{-1}$  at 0.1 A  $\text{g}^{-1}$  (508  $\text{mAh g}^{-1}$  at 2 A  $\text{g}^{-1}$  after 200 cycles). By comparison, the GNS-supported  $\text{Fe}_2\text{O}_3$  nanoparticle composite<sup>85</sup> obtained from the similar hydrothermal process in microwave oven exhibits better electrochemical properties with discharge capacities of 1,693, 1,142, 1,120, 1,098, and 1,027  $\text{mAh g}^{-1}$  in the first, tenth, 20th, 30th, and 50th cycles, respectively. A high capacity of ~800  $\text{mAh g}^{-1}$  is also observed at a current density of 800  $\text{mA g}^{-1}$ . Among the various GNS-supported  $\text{Fe}_3\text{O}_4$  composites,  $\text{Fe}_3\text{O}_4$  has a trend to form a particle or a porous particle morphology by the microwave-assisted technology.<sup>86–89</sup> As reported by Yu et al, a series of  $\text{Fe}_3\text{O}_4$ -GNS nanostructures were synthesized by a simple nonaqueous sol-gel approach in a single-mode microwave apparatus.<sup>88</sup> With different compositional ratios of  $\text{Fe}_3\text{O}_4$  and GNS, reaction temperature, and times, as well as the synthesis method (Hummer's method or modified Hummer's procedure) of GO reactant, the obtained  $\text{Fe}_3\text{O}_4$ -GNS composites exhibit different particle sizes on the surface of GNS. The cycling performances of GNS-supported  $\text{Fe}_3\text{O}_4$  composites are very stable even at high current



**Table 1** Summary on the morphologies and electrochemical performances of graphene-supported transitional metal oxide anodes

Composites	Morphologies	Electrochemical performances	Reference
3D Co <sub>3</sub> O <sub>4</sub> /GNS	Nanoparticle-on-sheet	An initial large discharge capacity of ~900 mAh g <sup>-1</sup> at 0.2 C, and the retained capacity of ~600 mAh g <sup>-1</sup> after 50 cycles	73
Co <sub>3</sub> O <sub>4</sub> /N-doped graphene	Nanoparticle-on-sheet	A reversible capacity of ~910 mAh g <sup>-1</sup> after 100 cycles at 100 mA g <sup>-1</sup>	74
Co <sub>3</sub> O <sub>4</sub> /GNS	Nanoparticle-on-sheet	A reversible capacity of ~1,785 mAh g <sup>-1</sup> after 90 cycles at 89 mA g <sup>-1</sup>	75
Co <sub>3</sub> O <sub>4</sub> /GNS	Nanoparticle-on-sheet	An initial large charge capacity of ~934 mAh g <sup>-1</sup> at 70 mA g <sup>-1</sup> and a high retained capacity of 650 mAh g <sup>-1</sup> after 50 cycles at 700 mA g <sup>-1</sup>	76
Co <sub>3</sub> O <sub>4</sub> /GNS	Sheet-on-sheet	An initial large charge capacity of ~1,235 mAh g <sup>-1</sup> at 89 mA g <sup>-1</sup> , and the retained capacity of ~1,065 mAh g <sup>-1</sup> after 30 cycles	77
CuO/RGO	Nanoparticle-on-sheet	An initial large discharge capacity of ~1,043 mAh g <sup>-1</sup> at 0.1 mA cm <sup>-2</sup> , and the retained capacity of ~516 mAh g <sup>-1</sup> after 45 cycles	78
CuO@Cu/RGO	Nanoparticle-on-sheet	An initial large charge capacity of ~734 mAh g <sup>-1</sup> at 50 mA g <sup>-1</sup> , and the retained capacity of ~842 mAh g <sup>-1</sup> after 50 cycles	79
CuO-Cu <sub>2</sub> O/GNS	Nanosphere-on-sheet	A reversible capacity of 487 mAh g <sup>-1</sup> retains after 60 cycles at 200 mA g <sup>-1</sup>	80
CuO/GNS	Nanowire-on-sheet	A reversible capacity of 770 mAh g <sup>-1</sup> retains after 100 cycles at 100 mA g <sup>-1</sup>	81
CuO/GNS	Sheet-on-sheet	An initial large charge capacity of ~1,092 mAh g <sup>-1</sup> at 70 mA g <sup>-1</sup> , and the retained capacity of ~801 mAh g <sup>-1</sup> after 40 cycles	82
CuO/GNS	Fusiform-on-sheet	An initial large charge capacity of ~956 mAh g <sup>-1</sup> at 70 mA g <sup>-1</sup> , and the retained capacity of ~666 mAh g <sup>-1</sup> after 40 cycles	82
CuO/GNS	Nanoleaf-on-sheet	A reversible capacity of 600 mAh g <sup>-1</sup> retains after 50 cycles at 100 mA g <sup>-1</sup>	83
Fe <sub>2</sub> O <sub>3</sub> /N-doped graphene	Nanorod-on-sheet	A stable capacity of 508 mAh g <sup>-1</sup> at 2 A g <sup>-1</sup> after 200 cycles, and an impressive capacity of 249 mAh g <sup>-1</sup> at 20 A g <sup>-1</sup> after 2,000 cycles without capacity fading	84
Fe <sub>2</sub> O <sub>3</sub> /RGO	Nanoparticle-on-sheet	An initial large charge capacity of ~1,227 mAh g <sup>-1</sup> at 100 mA g <sup>-1</sup> , and the retained capacity of ~1,027 mAh g <sup>-1</sup> after 50 cycles based on the mass of Fe <sub>2</sub> O <sub>3</sub>	85
Fe <sub>3</sub> O <sub>4</sub> /GNS	Nanoparticle-on-sheet	An initial large discharge capacity of ~1,320 mAh g <sup>-1</sup> at 0.1 C, and the retained capacity of ~650 mAh g <sup>-1</sup> after 50 cycles	86
Fe <sub>3</sub> O <sub>4</sub> /RGO	Nanoparticle-on-thin layer	A reversible capacity of 612 mAh g <sup>-1</sup> at 1 C, with a Coulombic efficiency of 98% after 50 cycles	87
Fe <sub>2</sub> O <sub>3</sub> /RGO	Nanoparticle-on-thin layer	A reversible capacity of 1,050 mAh g <sup>-1</sup> at 100 mA g <sup>-1</sup> , and a reversible capacity of 500 mAh g <sup>-1</sup> at 1,600 mA g <sup>-1</sup>	88
Fe <sub>2</sub> O <sub>3</sub> /GNS	Rice-on-sheet	An initial large discharge capacity of ~1,184 mAh g <sup>-1</sup> at 0.1 C, and the retained capacity of ~734 mAh g <sup>-1</sup> after 40 cycles	89
Fe <sub>2</sub> O <sub>3</sub> /GNS	Nanoparticle-on-sheet	An initial large discharge capacity of ~1,120 mAh g <sup>-1</sup> at 0.1 C, and the retained capacity of ~312 mAh g <sup>-1</sup> after 40 cycles	89
Mn <sub>3</sub> O <sub>4</sub> /GNS	Nanoparticle-on-sheet	A high reversible specific capacity of more than 900 mAh g <sup>-1</sup> at 40 mA g <sup>-1</sup> with no capacity decay up to 50 cycles	90
MoO <sub>3</sub> /GNS	Nanobelt-on-layer	A reversible capacity of 172 mAh g <sup>-1</sup> retained after 100 cycles at 100 mA g <sup>-1</sup>	91
MoO <sub>2</sub> /GNS	Nanoparticle-on-sheet	An initial large discharge capacity of ~1,296 mAh g <sup>-1</sup> at 0.1 C, and the retained capacity of ~1,330 mAh g <sup>-1</sup> after 100 cycles	92
ZnO/GNS	Nanocrystal-on-sheet	A reversible capacity of 460 mAh g <sup>-1</sup> retained after 50 cycles at 1 C	93

**Abbreviations:** GNS, graphene nanosheets; RGO, reduced graphene oxide.

density, which delivers high capacity of over 500 mAh g<sup>-1</sup> at 1,600 mA g<sup>-1</sup>.<sup>88</sup> Moreover, the Fe<sub>2</sub>O<sub>3</sub>-GNS rice-on-sheet and particle-on-sheet nanocomposites were synthesized by single-mode microwave hydrothermal technique with and without NH<sub>4</sub>H<sub>2</sub>PO<sub>4</sub>, respectively, as shown in Figure 4A.<sup>89</sup> The Fe<sub>2</sub>O<sub>3</sub> nanorice is observed with a length of 200 nm and diameters in the range of ~40 nm in the middle part to only 3–5 nm in the tip (Figure 4C), while the nanoparticle is nearly a nanocube-like morphology of ~50–80 nm in size (Figure 4B). The Fe<sub>2</sub>O<sub>3</sub>-GNS rice-on-sheet composite exhibits large reversible charge capacities of 825, 762, and 633 mAh g<sup>-1</sup> at large currents of 1, 2, and 5 C (1 C = 1,000 mA g<sup>-1</sup>) respectively. A high capacity

of 582 mAh g<sup>-1</sup> can be observed at 1 C after 100 cycles. The rice-on-sheet composite also shows more stable cycle life and better high-rate performance than the particle-on-sheet composite (Figure 4D and E).

There are also several reports on GNS-supported other transitional metal oxides. Their electrochemical performances are summarized in Table 1. GNS-supported Mn<sub>3</sub>O<sub>4</sub> particle composite was prepared by a microwave hydrothermal method.<sup>90</sup> It exhibits a high specific capacity of more than 900 mAh g<sup>-1</sup> at 40 mA g<sup>-1</sup> and no capacity fading up to 50 cycles. By a similar microwave hydrothermal process, the MoO<sub>3</sub> nanobelt/graphene film was also reported by

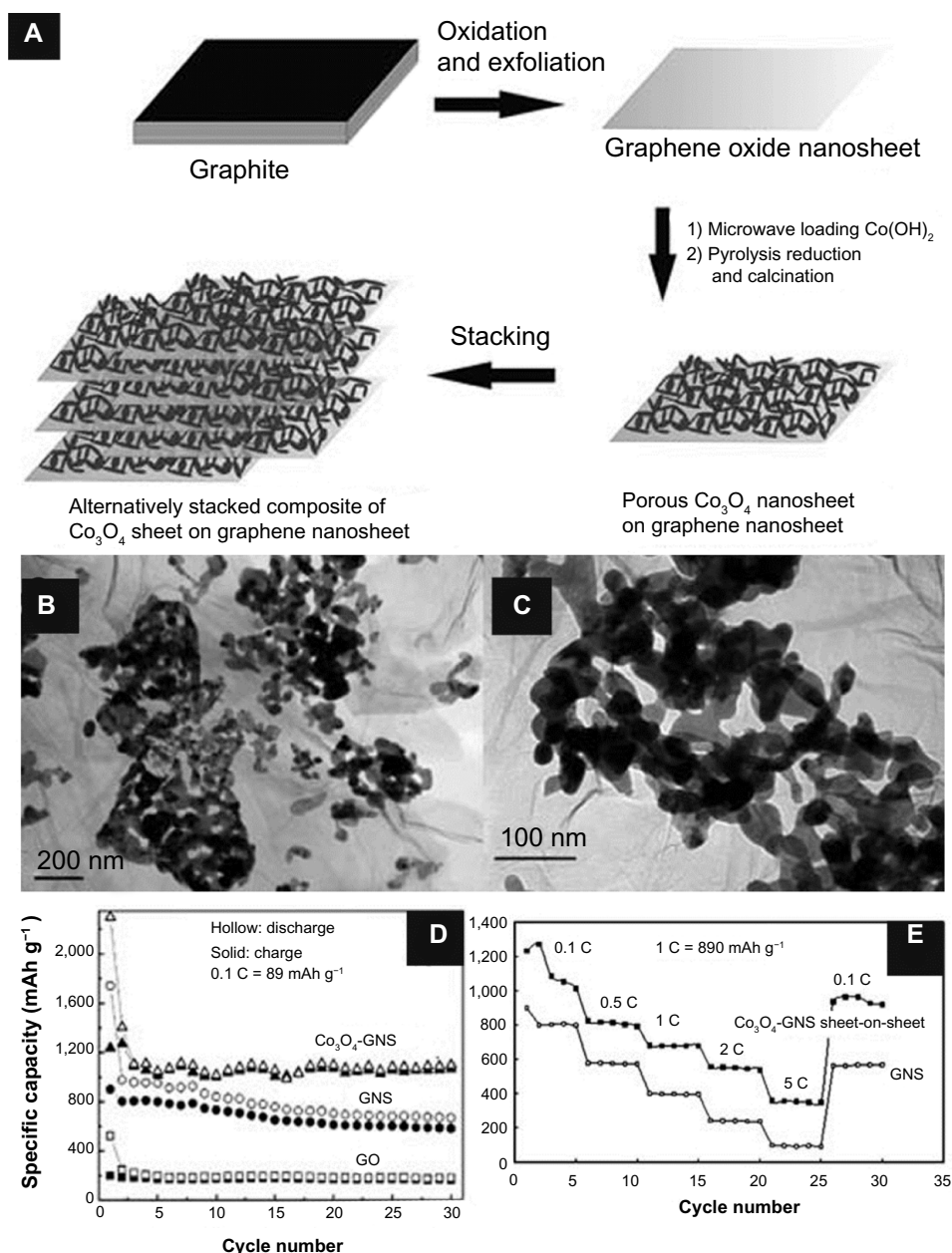


**Figure 2** The  $\text{Co}_3\text{O}_4$ -GNS composite and its electrochemical properties.

**Notes:** (A) Schematic illustration of the growth process, (B and C) TEM images, (D) cycling performances at 0.1 C (89  $\text{mAh g}^{-1}$ ) and (E) rate capability performances of  $\text{Co}_3\text{O}_4$ -GNS sheet-on-sheet composite. Reproduced from Chen SQ, Wang Y. Microwave-assisted synthesis of a  $\text{Co}_3\text{O}_4$ -graphene sheet-on-sheet nanocomposite as a superior anode material for Li-ion batteries. *J Mater Chem*. 2010;20:9735–9739, with permission from The Royal Society of Chemistry.<sup>77</sup>

**Abbreviations:** GNS, graphene nanosheet; GO, graphene oxide; TEM, transmission electron microscopy.

Noerchim et al<sup>91</sup> and exhibits initial discharge capacity of 291  $\text{mAh g}^{-1}$  at 100  $\text{mA g}^{-1}$  and 172  $\text{mAh g}^{-1}$  after 100 cycles. Moreover, 3D porous  $\text{MoO}_2$ /graphene microspheres were prepared in a microwave-assisted hydrothermal process. The obtained  $\text{MoO}_2$ /graphene composite exhibits excellent cycling stability of 1,300  $\text{mAh g}^{-1}$  after 80 cycles at 0.1 C and good rate capability of 913 and 390  $\text{mAh g}^{-1}$  at 2 and 5 C, respectively.<sup>92</sup> The  $\text{ZnO}@$ graphene composite<sup>93</sup> was synthesized from ZnO nanoparticles via a microwave-assisted

deposition on GO in a microwave oven. It exhibits improved electrochemical performance with a high capacity of 850  $\text{mAh g}^{-1}$  at 0.1 C. There is a small capacity decay of ~8% during 50 cycles of discharge and charge.

## GNS-supported tin/germanium/silicon based anodes

Tin, germanium and silicon are high-capacity elements for lithium storage, whose theoretical capacities values are 990,

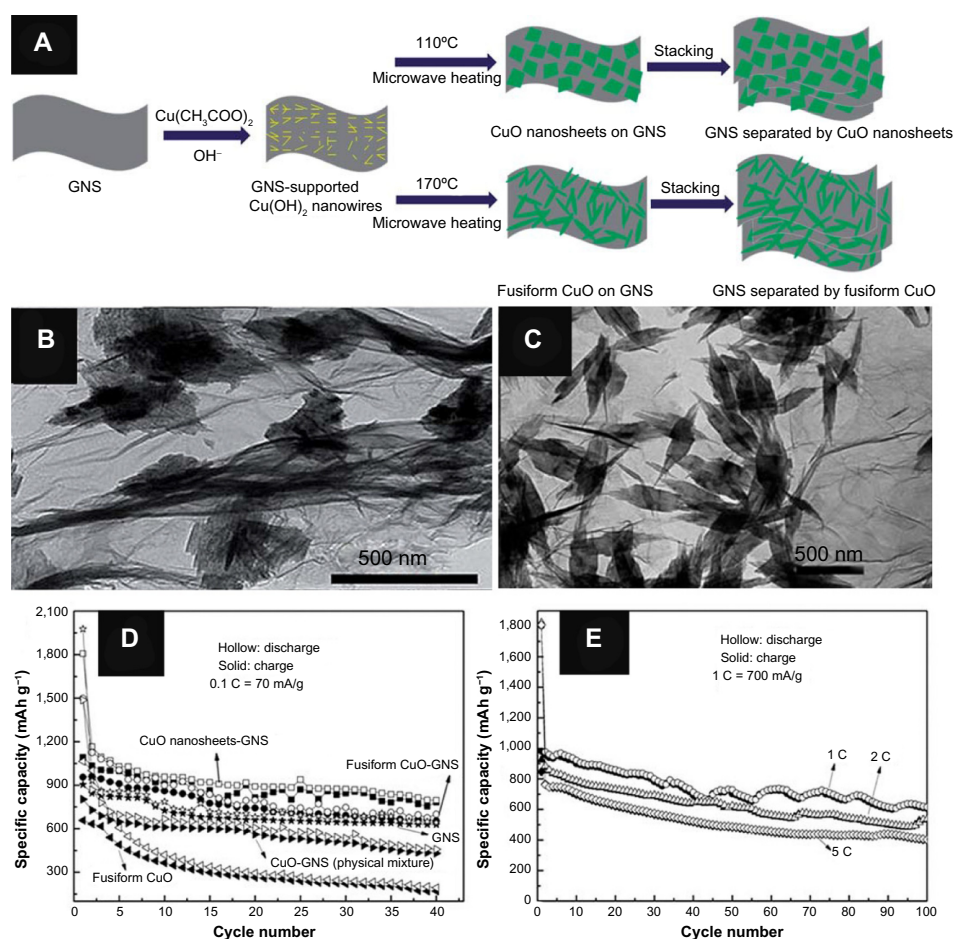


**Figure 3** The CuO-GNS composites and their electrochemical properties.

**Notes:** (A) Schematic illustration of the growth process of CuO-GNS sheet-on-sheet and fusiform-on-sheet structures, (B) TEM image of the CuO-GNS sheet-on-sheet composite, (C) TEM image of the CuO-GNS fusiform-on-sheet composite, (D) cycling performances at 0.1 C (70 mA g<sup>-1</sup>) for various CuO-GNS composites, (E) rate capability performances of the CuO-GNS sheet-on-sheet composite. Reproduced from Lu LQ, Wang Y. Sheet-like and fusiform CuO nanostructures grown on graphene by rapid microwave heating for high Li-ion storage capacities. *J Mater Chem*. 2011;21:17916–17921, with permission from The Royal Society of Chemistry.<sup>82</sup>

**Abbreviations:** GNS, graphene nanosheets; TEM, transmission electron microscopy.

1,600, and 4,200 mAh g<sup>-1</sup>, respectively. These theoretical values are calculated based on the lithium-ion reaction to form lithium alloys ( $\text{Li}_{4.4}\text{Sn}$ ,  $\text{Li}_{4.4}\text{Ge}$ , and  $\text{Li}_{4.4}\text{Si}$ ). It is worth noting that these elements are often used as oxides such as  $\text{SnO}$ ,  $\text{SnO}_2$ ,  $\text{GeO}_2$ , and  $\text{SiO}_2$ . The lithium ion can reduce these oxides to Sn, Ge, and Si at an early stage, followed by a similar lithium alloy and de-alloy storage mechanism. The oxygen element in these oxides is usually believed to be inactive for lithium ion storage. As summarized in Table 2, among the reported GNS-supported lithium alloy anodes by microwave-assisted technology,  $\text{Sn}^{94-98}$  or  $\text{SnO}_2^{99-106}$  usually tends to form a nanoparticle/nanocrystal morphology in the presence of GNS. GNS-supported Ge nanoparticle<sup>107</sup> or thin film<sup>108</sup> and GNS-supported Si nanoparticle<sup>109</sup> or thin film<sup>110</sup> was also synthesized by microwave irradiation or microwave plasma methods.

Figure 5A shows the schematic illustration of the preparation of graphene-supported Sn nanoparticles, which were

synthesized via a single-mode microwave hydrothermal process in a microwave reactor, followed by hydrogen gas reduction.<sup>95</sup> Figure 5B and C show the obtained GNS-supported Sn nanoparticles. Interestingly, the size of Sn nanoparticles in the Sn-GNS composite is changed from 60–120 nm (Sn-GNS-1) to 10–20 nm (Sn-GNS-2) when the ratio of Sn and GNS is reduced from 1:1 to 1:4. When used as the anode for LIBs, the Sn-GNS-1 and Sn-GNS-2 composites deliver reversible charge capacities of 1,206 and 1,407 mAh g<sup>-1</sup>, respectively, with the corresponding Coulombic efficiencies of 67.9% and 65.9%. As shown in the cycling performance curves of Figure 5D, the Sn-GNS-1 and Sn-GNS-2 electrodes deliver specific capacities of 772 and 1,100 mAh g<sup>-1</sup>, respectively, after 30 cycles at 0.1 C, which are both higher than that for bare GNS (582 mAh g<sup>-1</sup>) after the same cycle number. The enhanced high-rate properties are also observed for Sn-GNS-2, which exhibits specific



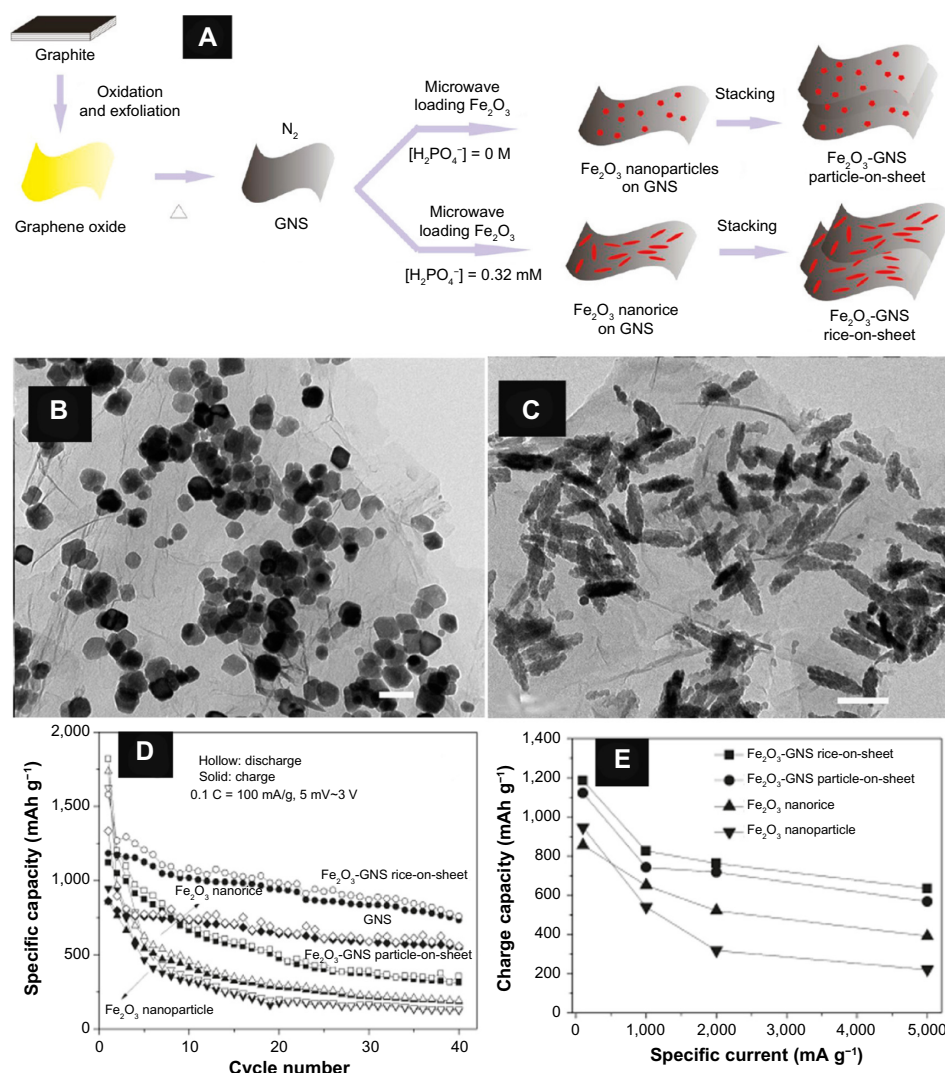


**Figure 4** The  $\text{Fe}_2\text{O}_3$ -GNS composites and their electrochemical properties.

**Notes:** (A) Schematic illustration of the growth process of  $\text{Fe}_2\text{O}_3$ -GNS particle-on-sheet and rice-on-sheet composites. TEM images of (B)  $\text{Fe}_2\text{O}_3$ -GNS particle-on-sheet and (C)  $\text{Fe}_2\text{O}_3$ -GNS rice-on-sheet composite. Electrochemical performances of  $\text{Fe}_2\text{O}_3$ -GNS composites: (D) cycling performances at 0.1 C (100  $\text{mA g}^{-1}$ ) and (E) rate capability. Reprinted with permission from Zou YQ, Kan J, Wang Y.  $\text{Fe}_2\text{O}_3$ -graphene rice-on-sheet nanocomposite for high and fast lithium ion storage. *J Phys Chem C*. 2011;115: 20747–20753. Copyright © 2011. American Chemical Society.<sup>89</sup>

**Abbreviations:** GNS, graphene nanosheets; TEM, transmission electron microscopy.

discharge capacities of 1,247, 1,106, 946, and 876  $\text{mAh g}^{-1}$  at current densities of 0.5, 1, 2, and 5 C. Moreover, a new strategy for the growth of self-assembled  $\text{Sn@CNT}$  on vertically aligned graphene (VAGN) was suggested by the microwave plasma irradiation method in MPCVD system.<sup>94</sup>  $\text{SnO}_2$  is reduced to Sn on VAGN and subsequently encapsulated in the catalyzed carbon nanotubes (CNTs). In the  $\text{Sn@CNT}$  product, pear-like Sn core with a diameter of about 30 nm and a length of 40–50 nm is encapsulated inside a cylindrical CNT with a length less than 100 nm. The whole  $\text{Sn@CNT}$  structure is anchored on the surface of GNS. Such a composite exhibits a high reversible capacity of 1,026  $\text{mAh g}^{-1}$  at 0.25 C, and a capacity of 140  $\text{mAh g}^{-1}$  is retained in a short discharge time of 12 seconds. A  $\text{Sn@graphene}$  on the

VAGN structure<sup>97</sup> was also reported by the same authors as above, which exhibits a reversible capacity of 1,005  $\text{mAh g}^{-1}$  at 0.25 C even after 120 cycles. Meanwhile, there are several other reports on GNS-supported  $\text{SnO}_2$  particles<sup>99–106</sup> prepared by microwave-assisted method. Excellent electrochemical properties (a stable capacity of  $\sim 890 \text{ mAh g}^{-1}$  without noticeable fading up to 80 cycles at 500  $\text{mA g}^{-1}$ ) were observed for the GNS- $\text{SnO}_2$  nanocomposite, which was synthesized by a microwave-assisted hydrothermal process.<sup>101</sup>

A unique sandwich-structured C/Ge/graphene composite<sup>107</sup> was synthesized by a microwave-solvothermal process as shown in Figure 6A. A carbon coating layer is introduced on the surface of the graphene/germanium oxide composite precursor, followed by a reduction treatment. The composite consists of



**Table 2** Summary on the morphologies and electrochemical performances of graphene-supported Sn/Ge/Si-based anodes

Composites	Morphologies	Electrochemical performances	Reference
Sn@CNTs-GNS	Nanoparticle-on-sheet	An initial large discharge capacity of $\sim 1,095 \text{ mAh g}^{-1}$ at $200 \text{ mA g}^{-1}$ , and the retained capacity of $\sim 1,013 \text{ mAh g}^{-1}$ after 200 cycles	94
Sn/GNS	Nanoparticle-on-sheet	Charge capacities of 1,206 and $1,407 \text{ mAh g}^{-1}$ with retained capacities of 772 and $1,100 \text{ mAh g}^{-1}$ after 30 cycles at $0.1 \text{ C}$ for Sn-GNS-1 and Sn-GNS-2, respectively	95
C-Sn/GNS	Nanoparticle-on-sheet	A stable capacity of $\sim 600 \text{ mAh g}^{-1}$ at $100 \text{ mA g}^{-1}$ with a higher capacity retention of 87% after 20 cycles	96
Sn/GNS	Nanoparticle-on-sheet	An initial large charge capacity of $\sim 1,035 \text{ mAh g}^{-1}$ at $150 \text{ mA g}^{-1}$ , and the retained capacity of $\sim 1,005 \text{ mAh g}^{-1}$ after 120 cycles	97
Sn/GNS	Nanoparticle-on-sheet	Discharge capacities of 1,300 and $730 \text{ mAh g}^{-1}$ after 40 cycles for as deposited and annealed Sn-GNS, respectively	98
$\text{SnO}_2/\text{GNS}$	Nanoparticle-on-sheet	Capacities between 400 and $500 \text{ mAh g}^{-1}$ after 80 cycles	99
$\text{SnO}_2/\text{GNS}$	Nanoparticle-on-sheet	Retained capacities of 590 and $504 \text{ mAh g}^{-1}$ after 200 cycles for $\text{SnO}_2\text{-GNS1}$ and $\text{SnO}_2\text{-GNS2}$ , respectively	100
$\text{SnO}_2/\text{GNS}$	Nanoparticle-on-sheet	A stable capacity of about $890 \text{ mAh g}^{-1}$ without noticeable fading up to 80 cycles at $500 \text{ mA g}^{-1}$	101
$\text{SnO}_2/\text{GNS}$	Nanocrystal-on-sheet	An initial large charge capacity of $\sim 1,329 \text{ mAh g}^{-1}$ at $100 \text{ mA g}^{-1}$ , and the retained capacity of $\sim 618 \text{ mAh g}^{-1}$ after 20 cycles	102
$\text{SnO}_2\text{-RGO-CNT}$	Nanoparticle-on-sheet	A reversible capacity of the composite retains $502 \text{ mAh g}^{-1}$ after 50 cycles at $100 \text{ mA g}^{-1}$ , and a capacity of $344 \text{ mAh g}^{-1}$ at $1,000 \text{ mA g}^{-1}$	103
$\text{SnO}_2/\text{GNS}$	Nanoparticle-on-sheet	An initial large charge capacity of $\sim 1,402 \text{ mAh g}^{-1}$ at $100 \text{ mA g}^{-1}$ , and the retained capacity of $\sim 1,359 \text{ mAh g}^{-1}$ after 100 cycles	104
$\text{SnO}_2/\text{GNS}$	Nanoparticle-on-sheet	A reversible capacity of $635 \text{ mAh g}^{-1}$ retains after 100 cycles at $60 \text{ mA g}^{-1}$	105
$\text{SnO}_2/\text{GNS}$	Nanoparticle-on-sheet	A stable specific capacity of about $430 \text{ mAh g}^{-1}$ retained after more than 140 cycles at $500 \text{ mA g}^{-1}$ with a Coulombic efficiency close to 100%	106
C-Ge-GNS	Nanoparticle-on-sheet	A reversible capacity of $993 \text{ mAh g}^{-1}$ retains after 160 cycles at $0.4 \text{ C}$	107
Ge/GNS	3D network	A reversible capacity of $1,140 \text{ mAh g}^{-1}$ at $0.33 \text{ C}$ over 100 cycles and $835 \text{ mAh g}^{-1}$ at $8 \text{ C}$ after 60 cycles	108
Si/GNS	Nanoparticle-on-sheet	Discharge capacity retention of about $800 \text{ mAh g}^{-1}$ after 100 cycles at a current of $500 \text{ mA g}^{-1}$	109
Si/GNS	Film-on-sheet	A capacity of $1,314 \text{ mAh g}^{-1}$ after 500 cycles with capacity retention of 84% relative to the maximum capacity of $1,560 \text{ mAh g}^{-1}$ in the 50th cycle	110
Ag/GNS	Nanoparticle-on-sheet	An initial large charge capacity of $\sim 780 \text{ mAh g}^{-1}$ at $0.1 \text{ C}$ , and the retained capacity of $\sim 714 \text{ mAh g}^{-1}$ after 50 cycles	111
Ag/GNS	Nanorod-on-sheet	A high reversible capacity of $1,015 \text{ mAh g}^{-1}$ at $0.1 \text{ C}$ with a high capacity retention rate of 64.1% at $5 \text{ C}$	112

**Abbreviations:** CNTs, carbon nanotubes; GNS, graphene nanosheets; RGO, reduced graphene oxide.

metallic germanium nanoparticles (20–30 nm in size) between graphene sheets and carbon layers (Figure 6B and C). The C/Ge/graphene composite shows better cycling performances (a capacity of  $993 \text{ mAh g}^{-1}$  after 160 cycles, corresponding to 86.4% of the capacity at the second cycle) and rate capability (discharge capacity of  $1,008 \text{ mAh g}^{-1}$  after 30 cycles at  $5 \text{ C}$ ) than the Ge/C and Ge/graphene composites.

3D graphene scaffold-supported Si thin film composite was prepared by Wang et al.<sup>110</sup> As shown in Figure 7A, a 3D graphene scaffold is first synthesized using a MPCVD approach, and Si is then deposited on the graphene scaffold using radio frequency sputtering. The obtained Si grains ( $0.3\text{--}0.5 \mu\text{m}$ ) are deposited on the surface of 3D graphene (Figure 7B). Figure 7C shows that these Si grains are composed of numerous Si nanoparticles (several

nanometers in size). When used for LIBs, such 3D graphene scaffold-supported Si electrode exhibits an outstanding cycling stability. A capacity of  $1,314 \text{ mAh g}^{-1}$  can be observed after 500 cycles with capacity retention of 84% relative to the maximum capacity of  $1,560 \text{ mAh g}^{-1}$  in the 50th cycle. The composite also exhibits good high-rate cycling performances and a large capacity of  $1,083 \text{ mAh g}^{-1}$  is still retained after 1,200 cycles at a large current of  $2.39 \text{ A g}^{-1}$ .

Based on the similar lithium alloy and de-alloy storage mechanism to Sn, Ge, and Si, Ag and Ag-based composites were also explored as the anodes for LIBs.<sup>111,112</sup> It is found in the literature that only GNS-supported Ag nanoparticle<sup>111</sup>/nanorod<sup>112</sup> composites were synthesized by microwave-assisted methods and their electrochemical properties are presented in Table 2. The Ag nanorod on GNS<sup>112</sup> is obtained

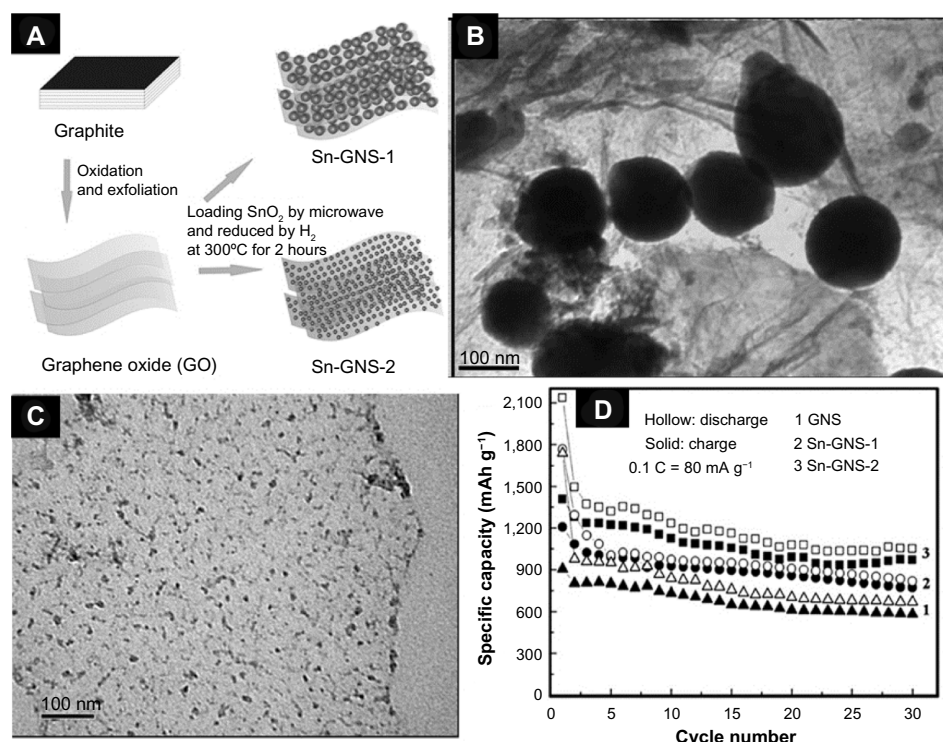


**Figure 5** The Sn-GNS composites and their electrochemical properties.

**Notes:** (A) Schematic illustration for the preparation process of Sn-GNS nanocomposites, (B) TEM images of Sn-GNS-1 (the weight ratios of Sn and GNS being 1:1), (C) TEM images of Sn-GNS-2 (the weight ratios of Sn and GNS being 1:4), (D) cycling performances of Sn-GNS composites at 80 mA g<sup>-1</sup>. Reprinted from *J Power Sources*, 216, Chen SQ, Wang Y, Ahn H, Wang GX, Microwave hydrothermal synthesis of high performance tin-graphene nanocomposites for lithium ion batteries, 22–27, Copyright © 2012 with permission from Elsevier.<sup>95</sup>

**Abbreviations:** GNS, graphene nanosheets; TEM, transmission electron microscopy.

by reducing Ag-GO hybrid. The Ag-GO precursor is prepared by two steps: Ag nanorods are first synthesized in a microwave solvothermal process in a household microwave oven and then mixed with GO prepared from Hummer's method. The Ag-GNS nanorod-on-sheet composite shows a high reversible capacity of 1,015 mAh g<sup>-1</sup> at 0.1 C with a high capacity retention rate of 64.1% at 5 C. By a similar microwave solvothermal process, GNS-Ag nanoparticle composite<sup>111</sup> was synthesized from natural graphite and silver salt, and it exhibits an initial charge capacity of 780 mAh g<sup>-1</sup>, which decreases to 714 mAh g<sup>-1</sup> after 50 cycles.

## GNS-supported metal sulfide anodes

Metal sulfides are also promising high-capacity anode materials for LIBs. The active element for lithium ions can be either metal (eg, Sn of SnS<sub>2</sub>) or sulfur (eg, S of CoS and NiS). Metal and sulfur are also suggested to be both active for In<sub>2</sub>S<sub>3</sub> materials, although most studies still believe the active element is only sulfur. The lithium ion storage mechanism of tin sulfide is similar to tin oxides, in which sulfide and oxygen are both inactive and lithium can reversibly react with tin to form Li<sub>x</sub>Sn alloys (the maximum x value is 4.4). The storage

mechanism of active sulfur element is based on the reversible formation and decomposition of lithium sulfide.

There are few reports on the GNS-supported metal sulfide composites with microwave-assisted syntheses: GNS-supported SnS<sub>2</sub> nanosheets,<sup>113</sup> SnS<sub>2</sub> nanoparticles,<sup>69</sup> In<sub>2</sub>S<sub>3</sub> particles and In<sub>2</sub>S<sub>3</sub> flowers<sup>114</sup> composites were reported by Chen et al, Zou and Wang, and Gu and Wang, respectively. Their morphologies and lithium-storage properties are summarized in Table 3. A porous 3D SnS<sub>2</sub>-reduced graphene oxide (RGO) sheet-on-sheet nanostructure was synthesized by a single-mode microwave solvothermal method at 180°C for 20 minutes in which SnS<sub>2</sub> nanosheets are distributed uniformly on the RGO surface.<sup>113</sup> If the amount of the starting GO is increased, the obtained SnS<sub>2</sub> products are only nanoparticles.<sup>69</sup> This is ascribed to the presence of a large amount of surface functionalities (mainly oxygen-containing groups) of GO, which can significantly affect the nucleation process of SnS<sub>2</sub>. As shown in Figure 8, large reversible capacities are observed from 1,077 to 896 mAh g<sup>-1</sup> at 0.1 C and 934 to 657 mAh g<sup>-1</sup> at 1 C in 40 cycles for the SnS<sub>2</sub>-RGO sheet-on-sheet composite. Compared with bare graphene and pristine SnS<sub>2</sub> nanoflowers, such a sheet-on-sheet composite achieves better electrochemical performances, which is attributed to the synergetic effect

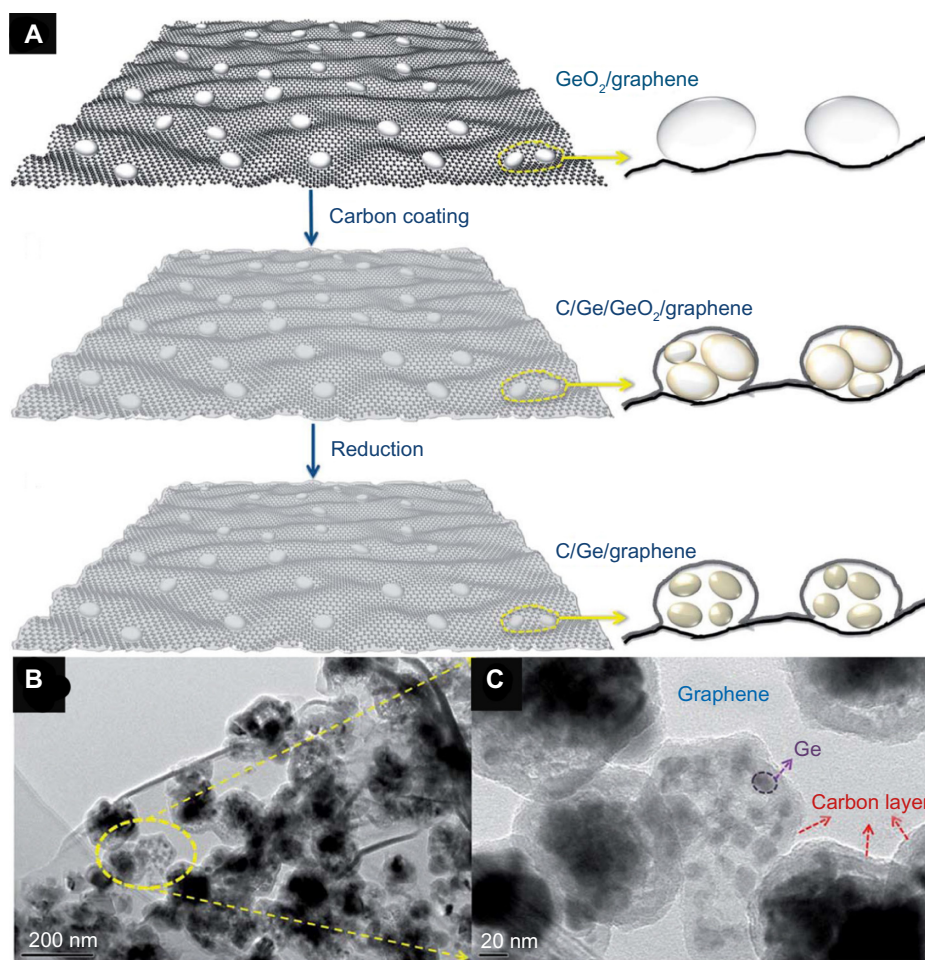


**Figure 6** The C/Ge/graphene composite.

**Notes:** (A) Schematic illustration of the C/Ge/graphene composite, (B and C) TEM images of C/Ge/graphene composite at different magnifications. Reproduced from Li D, Seng KH, Shi DQ, Chen ZX, Liu HK, Guo ZP. A unique sandwich-structured C/Ge/graphene nanocomposite as an anode material for high power lithium ion batteries. *J Mater Chem A*. 2013;1:14115–14121 with permission of The Royal Society of Chemistry.<sup>107</sup>

**Abbreviation:** TEM, transmission electron microscopy.

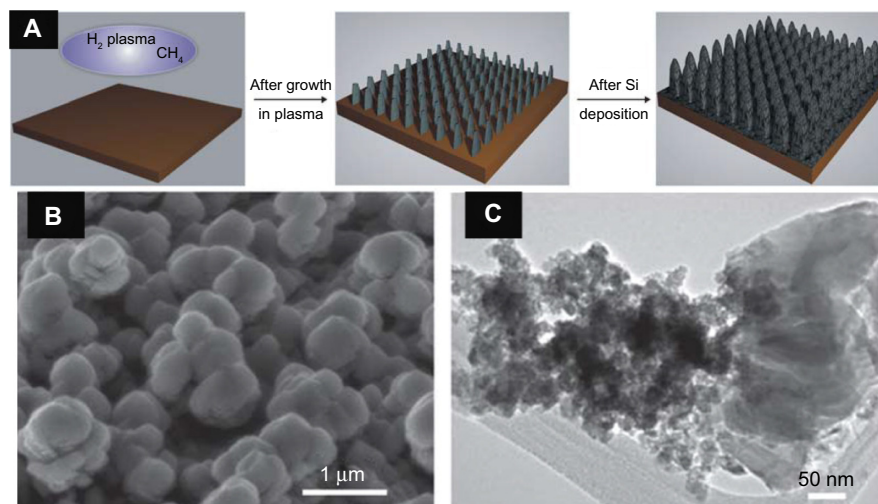


**Figure 7** The graphene supported Si composite.

**Notes:** (A) Schematic illumination of the growth process of the 3D graphene scaffold supported Si electrode (GSSSE). The as-synthesized GSSSE: (B) SEM image and (C) TEM image. Reproduced from Wang CD, Chui YS, Ma RG, et al. A three-dimensional graphene scaffold supported thin film silicon anode for lithium-ion batteries. *J Mater Chem A*. 2013;1:10092–10098 with permission of The Royal Society of Chemistry.<sup>110</sup>

**Abbreviations:** SEM, scanning electron microscopy; TEM, transmission electron microscopy.



**Table 3** Summary on the morphologies and electrochemical performances of graphene-supported metal sulfides and lithium titanium-based anodes

Composites	Morphologies	Electrochemical performances	Reference
SnS <sub>2</sub> /GNS	Sheet-on-sheet	Large reversible capacities of 1,077–896 mAh g <sup>-1</sup> at 0.1 C and 934–657 mAh g <sup>-1</sup> at 1 C in 40 cycles	113
In <sub>2</sub> S <sub>3</sub> /GNS	Flower-on-sheet	A reversible capacity of the composite retains 657 mAh g <sup>-1</sup> after 40 cycles at 70 mA g <sup>-1</sup>	114
In <sub>2</sub> S <sub>3</sub> /GNS	Particle-on-sheet	A reversible capacity of the composite retains 614 mAh g <sup>-1</sup> after 40 cycles at 70 mA g <sup>-1</sup>	114
Li <sub>4</sub> Ti <sub>5</sub> O <sub>12</sub> /GNS	Microsphere-on-sheet	Capacities of 168, 161, 153, 147, 143, 132, 119, and 106 mAh g <sup>-1</sup> at 0.2, 0.4, 1, 2, 4, 10, 20, and 40 C, respectively	115
Li <sub>4</sub> Ti <sub>5</sub> O <sub>12</sub> /RGO	Nanoparticle-on-sheet	A reversible capacity of 168 mAh g <sup>-1</sup> at 1 C with a high capacity retention rate of 59% at 50 C	116
Li <sub>4</sub> Ti <sub>5</sub> O <sub>12</sub> /RGO	Nanoplatelet-on-sheet	A discharge capacity of 154, 128, and 101 mAh g <sup>-1</sup> at 1, 50, and 100 C, respectively	117
TiO <sub>2</sub> /RGO	Microspheres-on-sheet	A large discharge capacity of 156 mAh g <sup>-1</sup> at 5 C, and 84 mAh g <sup>-1</sup> retained at 60 C	118

**Abbreviations:** GNS, graphene nanosheets; RGO, reduced graphene oxide.

for highly reversible lithium-ion storage that resulted from the closely contacted sheet-on-sheet morphology. These electrochemical properties of the sheet-on-sheet composite are also superior to previous SnS<sub>2</sub>-GNS particle-on-sheet composite<sup>69</sup> in which an initial charge capacity of 858 mAh g<sup>-1</sup> is decreased to 652 mAh g<sup>-1</sup> after 40 cycles.

GNS-supported In<sub>2</sub>S<sub>3</sub> nanoparticle and interconnected nanoflower composites were synthesized by the similar single-mode microwave hydrothermal method at 140°C under a pressure of 5.5 bars for 20 minutes.<sup>114</sup> Black powders of In<sub>2</sub>S<sub>3</sub>-graphene particle-on-sheet composite are obtained instead of the tawny powders of In<sub>2</sub>S<sub>3</sub>-graphene flower-on-sheet when the dosage of graphene is increased. As indicated by Figure 9, In<sub>2</sub>S<sub>3</sub> nanoparticles and nanoflowers are uniformly dispersed on GNS, forming sandwiched particle-on-sheet and unprecedented flower-on-sheet nanostructures. Compared with GNS and pristine In<sub>2</sub>S<sub>3</sub>, the GNS-supported In<sub>2</sub>S<sub>3</sub> composites show extraordinary large reversible capacities and good cycling performances. Reversible initial capacities of 1,249, 913, 782, and 690 mAh g<sup>-1</sup> are observed at currents of 70, 700, 1,400, 3,500 mA g<sup>-1</sup>, respectively, for the flower-on-sheet composite, while the particle-on-sheet composite shows slightly lower reversible capacities but more stable cycling performances at both small and high currents.

## Graphene-supported lithium titanium oxide based anodes

Lithium-titanium-oxide-based materials are important high-rate anodes for lithium ion batteries, which are based on the lithium insertion mechanism of lithium storage. Although their theoretical capacities are even lower than graphite anodes, they exhibit very good cyclabilities because there is only a small volume change during the process of lithium insertion and extraction. A summary of morphologies and electrochemical performances of graphene-supported lithium-titanium-

oxide-based anodes is given in Table 3. For example, Li<sub>4</sub>Ti<sub>5</sub>O<sub>12</sub> has been suggested as a zero-strain material with almost no structure change during cycling.<sup>115,116</sup> The microwave-hydrothermal method was reported to prepare Li<sub>4</sub>Ti<sub>5</sub>O<sub>12</sub> microspheres composed of nanoflakes wrapped in GNS.<sup>115</sup> The obtained structure can avoid the restacking of GNS and offer rapid lithium diffusion; therefore, the composite exhibits highly desirable Li-ion storage properties in terms of a large capacity (168 mAh g<sup>-1</sup> at 0.2 C) approaching the theoretical value, stable cycling performance, and excellent rate capability. The Li<sub>4</sub>Ti<sub>5</sub>O<sub>12</sub>/graphene composite was also prepared by the lithiation of the alkali titanate with the assistance of microwave.<sup>116</sup> The composite exhibits a reversible capacity of 168 mAh g<sup>-1</sup> at a current rate of 1 C with a high capacity retention rate of 59% at a very large current rate of 50 C. Kim et al also reported Li<sub>4</sub>Ti<sub>5</sub>O<sub>12</sub> nanoplatelet/RGO hybrid,<sup>117</sup> which was obtained from TiO<sub>2</sub>/RGO nano-hybrid in LiOH aqueous solution via a microwave hydrothermal process. The composite can deliver a discharge capacity of 154, 128, and 101 mAh g<sup>-1</sup> (based on Li<sub>4</sub>Ti<sub>5</sub>O<sub>12</sub>) at 1, 50, and 100 C, respectively. As reported by Yan et al, a facile microwave solvothermal process was developed to prepare an anatase TiO<sub>2</sub> anode material that maintains multiple properties including high surface area, high crystallinity, uniform mesoporous structure, perfect microspheres, and uniform particle size.<sup>118</sup> Using this fine anatase TiO<sub>2</sub> product, a TiO<sub>2</sub>/RGO hybrid material<sup>118</sup> was prepared under UV-light irradiation. The incorporation of RGO improves the electrochemical kinetics of the TiO<sub>2</sub> microspheres (Figure 10), which results in superior electrochemical performance in terms of specific capacity, rate capability, and cycle stability. The lithium storage mechanism of the anatase TiO<sub>2</sub> is also a lithium insertion mechanism. A reversible lithium insertion and extraction reaction between TiO<sub>2</sub> and Li<sub>0.5</sub>TiO<sub>2</sub> leads to a theoretical capacity of ~168 mAh g<sup>-1</sup>. The composite also shows a large discharge capacity of 156 mAh g<sup>-1</sup> at a large



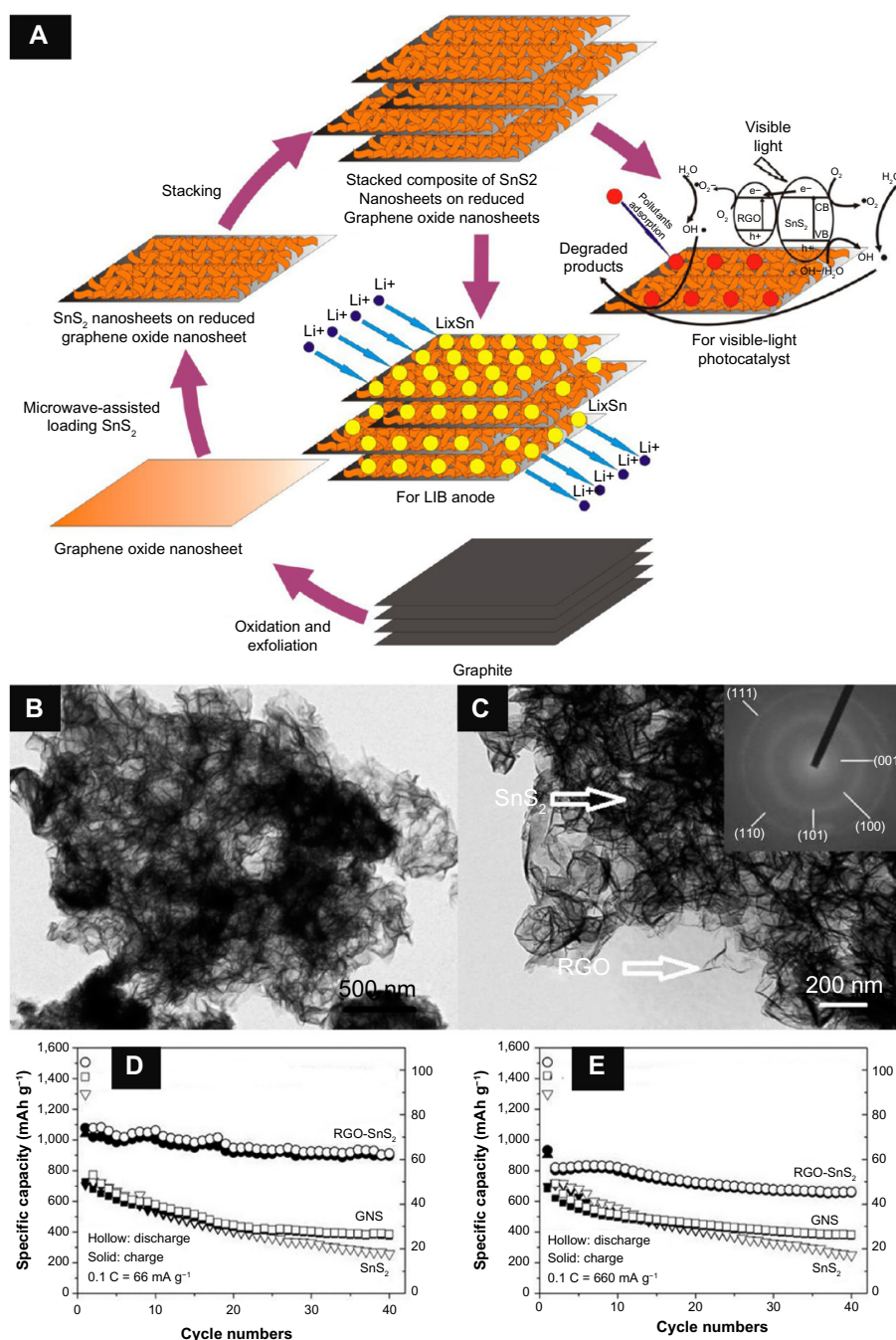


**Figure 8** The SnS<sub>2</sub>-GNS composite and its electrochemical properties.

**Notes:** (A) Schematic illustration of the growth process and applications of SnS<sub>2</sub>-RGO sheet-on-sheet nanostructure, (B and C) TEM images of SnS<sub>2</sub>-RGO sheet-on-sheet composite. The inset of (C) showing the selected area electronic diffraction (SAED) pattern of polycrystalline SnS<sub>2</sub>. Cycling performances of the products: (D) 0.1 C (66 mA g<sup>-1</sup>) and (E) 1 C. Reprinted with permission from Chen P, Su Y, Liu H, Wang Y. Interconnected tin disulfide nanosheets grown on graphene for Li-ion storage and photocatalytic applications. *ACS Appl Mater Interfaces*. 2013;5:12073–12082. Copyright © 2013. American Chemical Society.<sup>113</sup>

**Abbreviations:** LIB, lithium ion battery; RGO, reduced graphene oxide; TEM, transmission electron microscopy.

current rate of 5 C. Even at 60 C, a very high discharge capacity of 84 mAh g<sup>-1</sup> is still obtained.

## Other GNS composite anodes

In the literature, there are also some reports about other types of GNS-based anode composites. Kang et al reported

a CuCo<sub>2</sub>O<sub>4</sub>/RGO composite by a solvothermal reaction in a microwave reactor, followed by calcination treatment. Porous CuCo<sub>2</sub>O<sub>4</sub> nanocubes are well wrapped by RGO sheets.<sup>119</sup> Based on the observation of the Brunauer–Emmett–Teller (BET) results, the porous CuCo<sub>2</sub>O<sub>4</sub> nanocube/RGO composite exhibits a higher specific surface area (34.4 m<sup>2</sup> g<sup>-1</sup>)

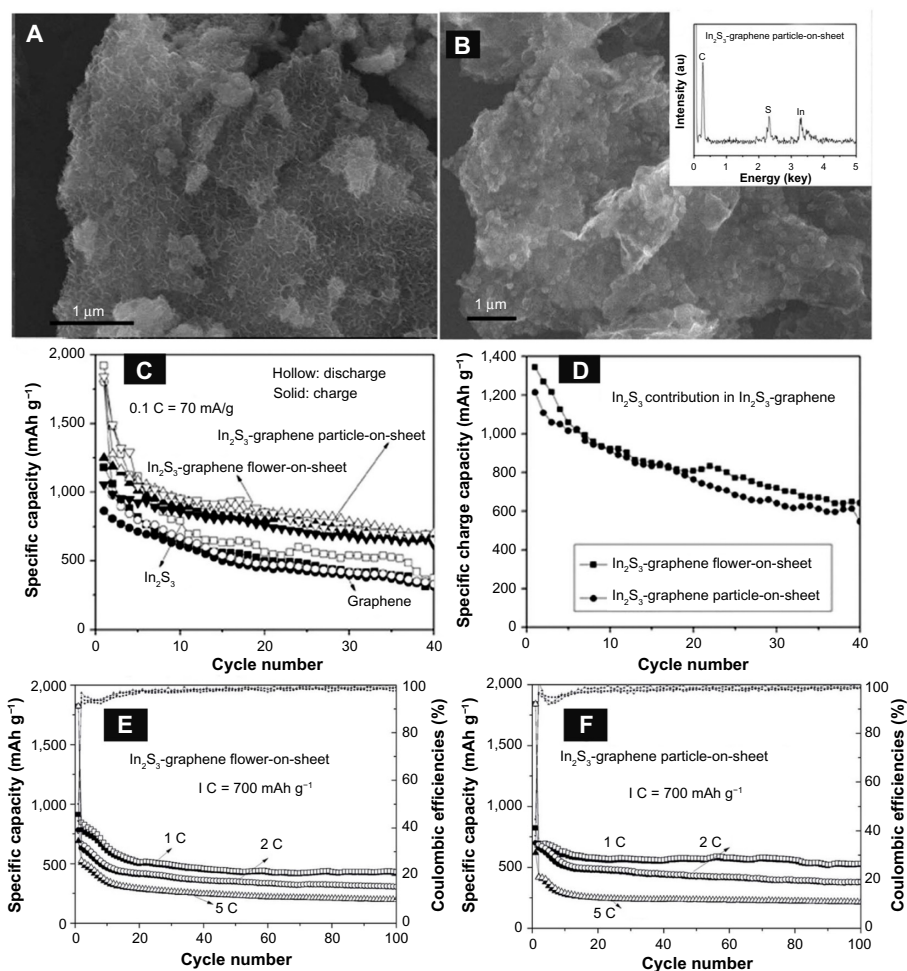


**Figure 9** The  $\text{In}_2\text{S}_3$ -GNS composites and their electrochemical properties.

**Notes:** (A) SEM image of the  $\text{In}_2\text{S}_3$ -GNS flower-on-sheet composite, (B) SEM image of the  $\text{In}_2\text{S}_3$ -GNS particle-on-sheet composite and the inset showing the energy-dispersive X-ray spectrum (EDS), (C) cycling performances at 0.1 C ( $70 \text{ mA g}^{-1}$ ) and (D)  $\text{In}_2\text{S}_3$  contribution in the composite. High-rate cycling performances: (E)  $\text{In}_2\text{S}_3$ -GNS flower-on-sheet and (F) particle-on-sheet composites at 1, 2, and 5 C. Reproduced from Gu Y, Wang Y. Microwave hydrothermal growth of  $\text{In}_2\text{S}_3$  interconnected nanoflowers and nanoparticles on graphene for high-performance Li-ion batteries. *RSC Adv.* 2014;4:8582–8589, with permission from The Royal Society of Chemistry.<sup>114</sup>

**Abbreviations:** au, arbitrary unit; GNS, graphene nanosheets; SEM, scanning electron microscopy.

than pristine  $\text{CuCo}_2\text{O}_4$  nanocubes ( $10.9 \text{ m}^2 \text{ g}^{-1}$ ). This would result in the increased contact areas between the electrode and the electrolyte solution when they are used as anodes for LIBs. Such a composite exhibits a high stable

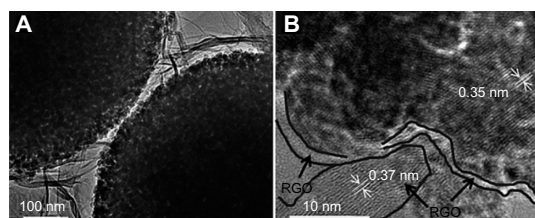


**Figure 10** The  $\text{TiO}_2/\text{RGO}$  composite.

**Notes:** (A) TEM image and (B) HRTEM image. Reproduced from Yan X, Li YJ, Du F, et al. Synthesis and optimizable electrochemical performance of reduced graphene oxide wrapped mesoporous  $\text{TiO}_2$  microspheres. *Nanoscale.* 2014;6:4108–4116 with permission from The Royal Society of Chemistry.<sup>118</sup>

**Abbreviations:** HRTEM, high resolution transmission electron microscopy; RGO, reduced graphene oxide; TEM, transmission electron microscopy.

capacity of  $\sim 570 \text{ mAh g}^{-1}$  at  $1,000 \text{ mA g}^{-1}$  after 350 cycles. Impressive high-rate performance is also observed (a high capacity of  $\sim 450 \text{ mAh g}^{-1}$  even at a high current density of  $5,000 \text{ mA g}^{-1}$ ). The morphologies and electrochemical properties of other graphene-based anode materials<sup>119–124</sup> for LIBs synthesized via similar microwave hydrothermal/solvothermal process in microwave oven/reactor are summarized in Table 4. Multilayer GNS were prepared by a microwave hydrothermal technique and then mixed with single-walled carbon nanotube by vacuum filtering.<sup>120</sup> The obtained free-standing GNS-single-walled carbon nanotube film exhibits a large  $d$ -spacing of  $0.41 \text{ nm}$  and a reversible capacity of  $\sim 300 \text{ mAh g}^{-1}$  during 50 cycles. Among these reports,<sup>119–124</sup> 3D GNS-CNT-Ni,<sup>123</sup> and GNS-CNT-Fe<sup>124</sup> composites show good lithium ion storage properties. They were both synthesized by similar microwave

**Table 4** Summary on the morphologies and electrochemical performances of other graphene-based anode materials

Composites	Morphologies	Electrochemical performances	Reference
CuCo <sub>2</sub> O <sub>4</sub> /RGO	Nanocube-on-sheet	An initial large charge capacity of ~540 mAh g <sup>-1</sup> at 1 A g <sup>-1</sup> , and the retained capacity of ~570 mAh g <sup>-1</sup> after 350 cycles	119
GNS-SWCNT	Free-standing film	An initial large charge capacity of 293 mAh g <sup>-1</sup> at 30 mA g <sup>-1</sup> , and the retained capacity of 303 mAh g <sup>-1</sup> after 50 cycles	120
RGO-CNT	3D network	An initial charge capacity of 682 mAh g <sup>-1</sup> at 50 mA g <sup>-1</sup> and the retained capacity of 298 mAh g <sup>-1</sup> after 50 cycles	121
Zn <sub>2</sub> GeO <sub>4</sub> /N-doped graphene	Nanorod-on-sheet	An initial charge capacity of 873 mAh g <sup>-1</sup> at 100 mA g <sup>-1</sup> and the retained capacity of 1,044 mAh g <sup>-1</sup> after 100 cycles with an excellent rate capability (531 mAh g <sup>-1</sup> at 3.2 A g <sup>-1</sup> )	122
3D GNS-CNT-Ni	3D network	An initial charge capacity of 1,089 mAh g <sup>-1</sup> at 100 mA g <sup>-1</sup> and the retained capacity of 648 mAh g <sup>-1</sup> after 50 cycles	123
3D GNS-CNT-Fe	3D network	A reversible capacity of ~1,024 mAh g <sup>-1</sup> after 40 cycles at 100 mA g <sup>-1</sup>	124

**Abbreviations:** CNT, carbon nanotube; GNS, graphene nanosheets; RGO, reduced graphene oxide; SWCNT, single-walled carbon nanotube.

hydrothermal method in a microwave oven/reactor, in which vertically aligned CNTs are grown directly on graphene sheets under the catalysis of Ni and Fe nanoparticles, respectively.

## GNS-decorated cathodes

Graphene is an active anode for LIBs within a comparatively low voltage window, however there is almost no lithium storage capacity for graphene at a higher voltage for cathode. Therefore graphene has been investigated with more research concerns as anodes for LIBs. In comparison, only a small amount of graphene is used for cathode composites with the purpose to improve the electrical conductivity of the cathode. And the GNS-decorated cathodes prepared by microwave-assisted methods are summarized with their morphologies and electrochemical properties in Table 5. Among various graphene-based cathodes by microwave irradiation, graphene-LiFePO<sub>4</sub> composite has attracted more interests.<sup>125–127</sup> As shown in Figure 11, a GNS-supported LiFePO<sub>4</sub> nanorod composite was synthesized by a novel one-pot microwave solvothermal process within 15 minutes at a temperature below 300°C in an microwave synthesis system.<sup>125</sup> The obtained graphene/LiFePO<sub>4</sub> nanohybrid exhibits a discharge capacity of ~164

mAh g<sup>-1</sup> (close to the theoretical value of 170 mAh g<sup>-1</sup>) at 0.1 C and good cyclability up to 70 cycles. LiFePO<sub>4</sub>/C/graphene composite was also reported by Shi et al.<sup>126</sup> After a rapid, one-pot, microwave-assisted hydrothermal method (15 minutes at 200°C), followed by sintering at 600°C for 2 hours under a H<sub>2</sub>/Ar (5:95, v/v) atmosphere, the obtained LiFePO<sub>4</sub> particles have sizes around 150 nm. These particles are wrapped in crumpled micrometer-size graphene sheets. The LiFePO<sub>4</sub>/C/graphene composite exhibits obviously improved electrochemical performance with highly stable reversible capacity of 88 mAh g<sup>-1</sup> at 10 C. Around 99% of the initial capacity can be retained after 40 cycles. Wang reported a similar LiFePO<sub>4</sub>/(C + graphene) structure.<sup>127</sup> The composite was obtained via a direct solid-state heating reaction in a microwave oven, which delivers a large discharge capacity (157.8 mAh g<sup>-1</sup>) at 0.1 C and more stable cycling performance than those of LiFePO<sub>4</sub>/C. A LiTi<sub>2</sub>(PO<sub>4</sub>)<sub>3</sub>/RGO particle-on-sheet composite was synthesized via microwave hydrothermal method in a microwave oven.<sup>128</sup> The particle-on-sheet composite can deliver a reversible capacity of 138 mAh g<sup>-1</sup> at 0.1 C, and over 93.2% of its initial capacity can be retained after 100 cycles at 1 C. With the similar microwave hydrothermal method, the LiMn<sub>2</sub>O<sub>4</sub>/RGO nanoparticle-on-sheet composite

**Table 5** Summary on the morphologies and electrochemical performances of graphene-decorated cathodes

Composites	Morphologies	Electrochemical performances	Reference
LiFePO <sub>4</sub> /GNS	Nanorod-on-sheet	A discharge capacity of ~164 mAh g <sup>-1</sup> at 0.1 C and good cyclability up to 70 cycles	125
LiFePO <sub>4</sub> /C/GNS	Nanoparticle-on-sheet	A high stable reversible capacity of 88 mAh g <sup>-1</sup> at 10 C and around 99% retained after 40 cycles	126
LiFePO <sub>4</sub> /C/GNS	Nanoparticle-on-sheet	A high initial discharge capacity of 157.8 mAh g <sup>-1</sup> at 0.1 C and 94.7 mAh g <sup>-1</sup> at 5.0 C	127
LiTi <sub>2</sub> (PO <sub>4</sub> ) <sub>3</sub> /RGO	Nanoparticle-on-sheet	A reversible capacity of 138 mAh g <sup>-1</sup> at 0.1 C, and retaining over 93.2% of its initial capacity after 100 cycles at 1 C	128
LiMn <sub>2</sub> O <sub>4</sub> /RGO	Nanoparticle-on-sheet	A high specific capacity of 137 mAh g <sup>-1</sup> at 1 C and a remarkably high discharge capacity of 117 mAh g <sup>-1</sup> and 101 mAh g <sup>-1</sup> at 50 and 100 C, respectively	129
FeF <sub>3</sub> /RGO	Nanoparticle-on-sheet	A stable capacity of 150 mAh g <sup>-1</sup> retained after 50 cycles	130

**Abbreviations:** GNS, graphene nanosheet; RGO, reduced graphene oxide.



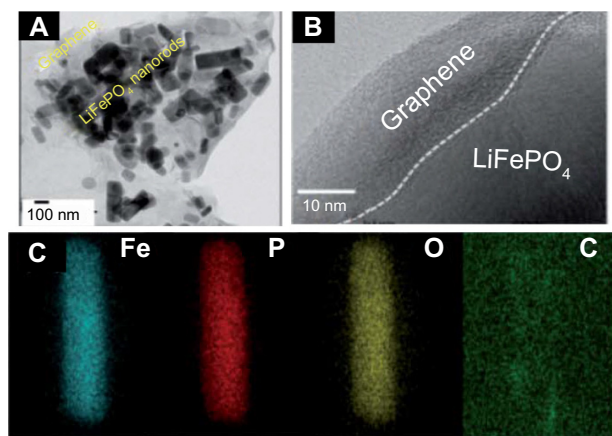


**Figure 11** The LiFePO<sub>4</sub>/GNS composite.

**Notes:** (A) TEM image, (B) HRTEM image, and (C) Elemental mapping images. Reproduced from Praneetha S, Murugan AV. A rapid, one-pot microwave-solvothermal synthesis of a hierarchical nanostructured graphene/LiFePO<sub>4</sub> hybrid as a high performance cathode for lithium ion batteries. *RSC Adv.* 2013;3:25403–25409 with permission of The Royal Society of Chemistry.<sup>125</sup>

**Abbreviations:** HRTEM, high resolution transmission electron microscopy; GNS, graphene nanosheets; TEM, transmission electron microscopy.

was obtained.<sup>129</sup> The composite can deliver a high specific capacity of 137 mAh g<sup>-1</sup> at 1 C and a remarkably high discharge capacity of 117 mAh g<sup>-1</sup> and 101 mAh g<sup>-1</sup> at 50 and 100 C, respectively. Moreover, a FeF<sub>3</sub>/RGO composite exhibits a nanoparticle-on-sheet morphology by a microwave solvothermal process.<sup>130</sup> It delivers a stable capacity of 150 mAh g<sup>-1</sup> after 50 cycles when used as a cathode for LIBs.

## Conclusion

Microwave synthesis has been demonstrated as a fast, uniform, energy-efficient, and scalable approach to prepare graphene-supported various electrodes. Representative examples such as graphene-supported transitional metal oxides, metal sulfide, tin/germanium/silicon/lithium titanium oxide based anodes, graphene-decorated lithium iron phosphate based cathodes, and some other graphene-based composite electrodes have been discussed. The fast microwave heating offers homogeneous reaction environment and leads to good control of shape, size, size distribution, and agglomeration of the products. The surface functionalities on graphene can be controlled to different extents and the introduced second-phase component to graphene can be also tuned with 0D, 1D, 2D morphologies, and their stacked 3D network. These graphene-based composites usually exhibit strong synergetic effect when used for LIBs. They deliver larger capacity and better cyclability and high-rate performance compared to individual component of the composite. These improved electrochemical properties have been attributed to the preserved promising properties of graphene and the improved electrical conductivity and more

stable mechanical structure of graphene-supported materials. These synthesized graphene composites with the assistance of microwave irradiation may find wide applications for other energy-storage applications such as supercapacitors and fuel cells. Furthermore, the microwave-assisted technology would be used more and more in the recent future to synthesize materials with controlled size and shape for the energy-storage application due to its simple, quick, inexpensive, uniform, and energy-efficient advantages.

## Acknowledgments

The authors gratefully acknowledge the follow-up Program for Professor of Special Appointment in Shanghai (Eastern Scholar), the National Natural Science Foundation of China (51271105 and 51201095), Shanghai Municipal Education Commission (13YZ012) and Innovative Research Team (IRT13078) for financial support. The authors also thank Lab for Microstructure, Instrumental Analysis and Research Center, Shanghai University, for materials characterizations.

## Disclosure

The authors report no conflicts of interest in this work.

## References

- Kim H, Hong J, Park KY, Kim H, Kim SW, Kang K. Aqueous rechargeable Li and Na ion batteries. *Chem Rev.* 2014;114:11788–11827.
- Mai LQ, Tian XC, Xu X, Chang L, Xu L. Nanowire electrodes for electrochemical energy storage devices. *Chem Rev.* 2014;114:11828–11862.
- Wang XF, Lu XH, Liu B, Chen D, Tong YX, Shen GZ. Flexible energy-storage devices: design consideration and recent progress. *Adv Mater.* 2014;26:4763–4782.
- Wang CW, Wang Y, Graser J, Zhao R, Gao F, O'Connell MJ. Solution-based carbohydrate synthesis of individual solid, hollow, and porous carbon nanospheres using spray pyrolysis. *ACS Nano.* 2013;7:11156–11165.
- Xia XH, Zhang YQ, Chao DL, et al. Solution synthesis of metal oxides for electrochemical energy storage applications. *Nanoscale.* 2014;6:5008–5048.
- Mahmood N, Zhang CZ, Liu F, Zhu JH, Hou YL. Hybrid of Co<sub>3</sub>Sn<sub>2</sub>@Co nanoparticles and nitrogen-doped graphene as a lithium ion battery anode. *ACS Nano.* 2013;7:10307–10318.
- Gu Y, Wu FD, Wang Y. Confined volume change in Sn-Co-C ternary tube-in-tube composites for high-capacity and long-life lithium storage. *Adv Funct Mater.* 2013;23:893–899.
- Zhang QF, Uchaker E, Candelaria SL, Cao GZ. Nanomaterials for energy conversion and storage. *Chem Soc Rev.* 2013;42:3127–3171.
- Zhu JX, Yang D, Yin ZY, Yan QY, Zhang H. Graphene and graphene-based materials for energy storage applications. *Small.* 2014;10:3480–3498.
- Wang DN, Yang JL, Li XF, et al. Layer by layer assembly of sandwiched graphene/SnO<sub>2</sub> nanorod/carbon nanostructures with ultrahigh lithium ion storage properties. *Energy Environ Sci.* 2013;6:2900–2906.
- Liang MH, Zhi LJ. Graphene-based electrode materials for rechargeable lithium batteries. *J Mater Chem.* 2009;19:5871–5878.
- Zhi J, Cui HL, Chen A, Xie Y, Huang FQ. Efficient highly flexible dye sensitized solar cells of three dimensional graphene decorated titanium dioxide nanoparticles on plastic substrate. *J Power Sources.* 2015;281:404–410.



13. Chang QH, Huang L, Wang JZ, et al. Nanoarchitecture of variable sized graphene nanosheets incorporated into three-dimensional graphene network for dye sensitized solar cells. *Carbon*. 2015;85:185–193.
14. Selopal GS, Milan R, Ortolani L, et al. Graphene as transparent front contact for dye sensitized solar cells. *S Energy Mat Sol C*. 2015;135:99–105.
15. Liu CG, Yu ZN, Neff D, Zhamu A, Jang BZ. Graphene-based supercapacitor with an ultrahigh energy density. *Nano Lett*. 2010;10:4863–4868.
16. Ge CY, Hou ZH, He BH, et al. Three-dimensional flower-like nickel oxide supported on graphene sheets as electrode material for supercapacitors. *J Solgel Sci Technol*. 2012;63:146–152.
17. Qu BH, Chen YJ, Zhang M, et al. b-Cobalt sulfide nanoparticles decorated graphene composite electrodes for high capacity and power supercapacitors. *Nanoscale*. 2012;4:7810–7816.
18. Zeng L, Zhao TS, An L, Zhao G, Yan XH, Jung CY. Graphene-supported platinum catalyst prepared with ionomer as surfactant for anion exchange membrane fuel cells. *J Power Sources*. 2015;275:506–515.
19. Liu Y, Jin XJ, Dionysiou DD, Liu H, Huang YM. Homogeneous deposition-assisted synthesis of iron-nitrogen composites on graphene as highly efficient non-precious metal electrocatalysts for microbial fuel cell power generation. *J Power Sources*. 2015;278:773–781.
20. Das D, Ghosh S, Basumallick I. Electrochemical studies on glucose oxidation in an enzymatic fuel cell with enzyme immobilized on to reduced graphene oxide surface. *Electroanalysis*. 2014;26:2408–2418.
21. Cueto M, Ocón P, Poyato JML. Comparative study of oxygen reduction reaction mechanism on nitrogen, phosphorus, and boron-doped graphene surfaces for fuel cell applications. *J Phys Chem C*. 2015;119:2004–2009.
22. Stankovich S, Dikin DA, Dommett GHB, et al. Graphene-based composite materials. *Nature*. 2006;442:282–286.
23. Li XF, Hu YH, Liu J, Lushington A, Li RY, Sun XL. Structurally tailored graphene nanosheets as lithium ion battery anodes: an insight to yield exceptionally high lithium storage performance. *Nanoscale*. 2013;5:12607–12615.
24. Wang J, Feng CQ, Sun ZQ, Chou SL, Liu HK, Wang JZ. In-situ one-step hydrothermal synthesis of a lead germanate-graphene composite as a novel anode material for lithium-ion batteries. *Sci Rep*. 2014;4:7030.
25. Vargas O, Caballero Á, Morales J, Elia GA, Scrosati B, Hassoun J. Electrochemical performance of a graphene nanosheets anode in a high voltage lithium-ion cell. *Phys Chem Chem Phys*. 2013;15:20444–20446.
26. Ye MH, Dong ZL, Hu CG, et al. Uniquely arranged graphene-on-graphene structure as a binder-free anode for high-performance lithium-ion batteries. *Small*. 2014;10:5035–5041.
27. Chen SQ, Chen P, Wang Y. Carbon nanotubes grown in situ on graphene nanosheets as superior anodes for Li-ion batteries. *Nanoscale*. 2011;3:4323–4329.
28. Geng H, Kong SF, Wang Y. NiS nanorod-assembled nanoflowers grown on graphene: morphology evolution and Li-ion storage applications. *J Mater Chem A*. 2014;2:15152–15158.
29. Sun WW, Wang Y. Graphene-based nanocomposite anodes for lithium-ion batteries. *Nanoscale*. 2014;6:11528–11532.
30. Ye JC, Charnvanichborikarn S, Worsley MA, Kucheyev SO, Wood BC, Wang YM. Enhanced electrochemical performance of ion-beam-treated 3D graphene aerogels for lithium ion batteries. *Carbon*. 2015;85:269–278.
31. Cai MZ, Thorpe D, Adamson DH, Schniepp HC. Methods of graphite exfoliation. *J Mater Chem*. 2012;22:24992–25002.
32. Alessandro HA, Videla M, Ban S, Specchia S, Zhang L, Zhang JJ. Non-noble Fe-NX electrocatalysts supported on the reduced graphene oxide for oxygen reduction reaction. *Carbon*. 2014;76:386–400.
33. Pham VH, Hur SH, Kim EJ, Kim BS, Chung JS. Highly efficient reduction of graphene oxide using ammonia borane. *Chem Commun*. 2013;49:6665–6667.
34. Pokharel P, Truong QT, Lee DS. Multi-step microwave reduction of graphite oxide and its use in the formation of electrically conductive graphene/epoxy composites. *Compos Part B Eng*. 2014;64:187–193.
35. Wong CHA, Jankovský O, Sofer Z, Pumera M. Vacuum-assisted microwave reduction/exfoliation of graphite oxide and the influence of precursor graphite oxide. *Carbon*. 2014;77:508–517.
36. Shulga YM, Baskakov SA, Knerelman EI, et al. Carbon nanomaterial produced by microwave exfoliation of graphite oxide: new insights. *RSC Adv*. 2014;4:587–592.
37. Chandrasekaran S, Ramanathan S, Basak T. Microwave food processing – A review. *Food Res Int*. 2013;52:243–261.
38. Abubakar Z, Salema AA, Ani FN. A new technique to pyrolyse biomass in a microwave system: effect of stirrer speed. *Bioresour Technol*. 2013;128:578–585.
39. Motasemi F, Afzal MT. A review on the microwave-assisted pyrolysis technique. *Renew Sust Energ Rev*. 2013;28:317–330.
40. Mutyal S, Fairbridge C, Paré JRJ, Bélanger JMR, Ng S, Hawkins R. Microwave applications to oil sands and petroleum: a review. *Fuel Process Technol*. 2010;91:127–135.
41. Faraji S, Ani FN. Microwave-assisted synthesis of metal oxide/hydroxide composite electrodes for high power supercapacitors – A review. *J Power Sources*. 2014;263:338–360.
42. Vázquez E, Giacalone F, Prato M. Non-conventional methods and media for the activation and manipulation of carbon nanoforms. *Chem Soc Rev*. 2014;43:58–69.
43. Boxall DL, Lukehart CM. Rapid synthesis of Pt or Pd/carbon nanocomposites using microwave irradiation. *Chem Mater*. 2001;13:806–810.
44. Gallis KW, Landry CC. Rapid calcination of nanostructured silicate composites by microwave irradiation. *Adv Mater*. 2001;13:23–26.
45. Liang J, Deng ZX, Jiang X, Li FL, Li YD. Photoluminescence of tetragonal ZrO<sub>2</sub> nanoparticles synthesized by microwave irradiation. *Inorg Chem*. 2002;41:3602–3604.
46. Patra CR, Alexandra G, Patra S, et al. Microwave approach for the synthesis of rhabdophane-type lanthanide orthophosphate (Ln = La, Ce, Nd, Sm, Eu, Gd and Tb) nanorods under solvothermal conditions. *New J Chem*. 2005;29:733–739.
47. Zlotorzynski A. The application of microwave radiation to analytical and environmental chemistry. *Crit Rev in Anal Chem*. 1995;25:43–76.
48. Datta AK, Davidson PM. Microwave and radio frequency processing. *J Food Sci*. 2000;65:32–41.
49. Murugan AV, Muraliganth T, Manthiram A. Rapid, facile microwave-solvothermal synthesis of graphene nanosheets and their polyaniline nanocomposites for energy storage. *Chem Mater*. 2009;21:5004–5006.
50. Hummers WS, Offeman RE. Preparation of graphitic oxide. *J Am Chem Soc*. 1958;80:1339–1339.
51. Wang Y, Liu G, An CH, et al. Bimetallic NiCo functional graphene: an efficient catalyst for hydrogen-storage properties of MgH<sub>2</sub>. *Chem Asian J*. 2014;9:2576–2583.
52. Chen WF, Yan LF, Bangal PR. Preparation of graphene by the rapid and mild thermal reduction of graphene oxide induced by microwaves. *Carbon*. 2010;48:1146–1152.
53. Hassan MAH, Abdelsayed V, Khder AERS, et al. Microwave synthesis of graphene sheets supporting metal nanocrystals in aqueous and organic media. *J Mater Chem*. 2009;19:3832–3837.
54. Wu ZS, Ren WC, Gao LB, Liu BL, Jiang CB, Cheng HM. Synthesis of high-quality graphene with a pre-determined number of layers. *Carbon*. 2009;47:493–499.
55. Shanmugaraj AM, Choi WS, Lee CW, Ryu SH. Electrochemical performances of graphene nanosheets prepared through microwave radiation. *J Power Sources*. 2011;196:10249–10253.
56. Sridhar V, Jeon JH, Oh IK. Synthesis of graphene nano-sheets using eco-friendly chemicals and microwave radiation. *Carbon*. 2010;48:2953–2957.
57. Khai TV, Kwak DS, Kwon YJ, et al. Direct production of highly conductive graphene with a low oxygen content by a microwave-assisted solvothermal method. *Chem Eng J*. 2013;232:346–355.
58. Malesevic A, Vitchev R, Schouteden K, et al. Synthesis of few-layer graphene via microwave plasma-enhanced chemical vapour deposition. *Nanotechnology*. 2008;19:305604.

59. Yuan GD, Zhang WJ, Yang Y, et al. Graphene sheets via microwave chemical vapor deposition. *Chem Phys Lett*. 2009;467:361–364.
60. Dato A, Radmilovic V, Lee Z, Phillips J, Frenklach M. Substrate-free gas-phase synthesis of graphene sheets. *Nano Lett*. 2008;8(7):2012–2016.
61. Fan X, Peng W, Li Y, et al. Deoxygenation of exfoliated graphite oxide under alkaline conditions: a green route to graphene preparation. *Adv Mater*. 2008;20:4490–4493.
62. Zhou Y, Bao QL, Tang LAL, Zhong YL, Loh KP. Hydrothermal dehydration for the “green” reduction of exfoliated graphene oxide to graphene and demonstration of tunable optical limiting properties. *Chem Mater*. 2009;21:2950–2956.
63. Long J, Fang M, Chen GH. Microwave-assisted rapid synthesis of water-soluble graphene. *J Mater Chem*. 2011;21:10421–10425.
64. Sridhar V, Lee I, Yoon HS, Chun HH, Park H. Microwave synthesis of three dimensional graphene-based shell-plate hybrid nanostructures. *Carbon*. 2013;61:633–639.
65. Liu XX, Zhan D, Chao DL, et al. Microwave-assisted production of giant graphene sheets for high performance energy storage applications. *J Mater Chem A*. 2014;2:12166–12170.
66. Eng AYS, Sofer Z, Šimek P, Kosina J, Pumera M. Highly hydrogenated graphene through microwave exfoliation of graphite oxide in hydrogen plasma: towards electrochemical applications. *Chem Eur J*. 2013;19:15583–15592.
67. Abdelsayed V, Panda AB, Glaspell GP, El-Shall MS. Synthesis, passivation, and stabilization of nanoparticles, nanorods, and nanowires by microwave irradiation. In: Nagarajan R, Hatton TA, editors. *Nanoparticles: Synthesis, Stabilization, Passivation, and Functionalization*. Washington, DC: American Chemical Society; 2009:225–247.
68. Thomas R, Rao KY, Rao GM. Morphology and electrochemical performance of graphene nanosheet array for Li-ion thin film battery. *Electrochim Acta*. 2013;108:458–464.
69. Zou YQ, Wang Y. Sn@CNT nanostructures rooted in graphene with high and fast Li-storage capacities. *ACS Nano*. 2011;5(10):8108–8114.
70. Gerbec JA, Magana D, Washington A, Strouse GF. Microwave-enhanced reaction rates for nanoparticle synthesis. *J Am Chem Soc*. 2005;127:15791–15800.
71. Panda AB, Glaspell G, El-Shall MS. Microwave synthesis of highly aligned ultra narrow semiconductor rods and wires. *J Am Chem Soc*. 2006;128:2790–2791.
72. Panda AB, Glaspell G, El-Shall MS. Microwave synthesis and optical properties of uniform nanorods and nanoplates of rare earth oxides. *J Phys Chem C*. 2007;111:1861–1864.
73. Sun F, Huang K, Qi X, et al. Enhanced 3D hierarchical double porous  $\text{Co}_3\text{O}_4$ /graphene architecture for superior rechargeable lithium ion battery. *Ceram Int*. 2014;40:2523–2528.
74. Lai LF, Zhu JX, Li ZG, et al.  $\text{Co}_3\text{O}_4$ /nitrogen modified graphene electrode as Li-ion battery anode with high reversible capacity and improved initial cycle performance. *Nano Energy*. 2014;3:134–143.
75. Zhou XY, Shi JJ, Liu Y, Su QM, Zhang J, Du GH. Microwave irradiation synthesis of  $\text{Co}_3\text{O}_4$  quantum dots/graphene composite as anode materials for Li-ion battery. *Electrochim Acta*. 2014;143:175–179.
76. Hsieh CT, Lin JS, Chen YF, Teng H. Pulse microwave deposition of cobalt oxide nanoparticles on graphene nanosheets as anode materials for lithium ion batteries. *J Phys Chem C*. 2012;116:15251–15258.
77. Chen SQ, Wang Y. Microwave-assisted synthesis of a  $\text{Co}_3\text{O}_4$ -graphene sheet-on-sheet nanocomposite as a superior anode material for Li-ion batteries. *J Mater Chem*. 2010;20:9735–9739.
78. Rai AK, Anh LT, Gim J, et al. Facile approach to synthesize CuO/reduced graphene oxide nanocomposite as anode materials for lithium-ion battery. *J Power Sources*. 2013;244:435–441.
79. Li N, Xiao Y, Hu CW, Cao MH. Microwave-assisted synthesis of dual-conducting  $\text{Cu}_2\text{O}$ @Cu-graphene system with improved electrochemical performance as anode material for lithium batteries. *Chem Asian J*. 2013;8:1960–1965.
80. Zhou XY, Shi JJ, Liu Y, Su QM, Zhang J, Du GH. Microwave-assisted synthesis of hollow  $\text{CuO}$ - $\text{Cu}_2\text{O}$  nanosphere/graphene composite as anode for lithium-ion battery. *J Alloy Compd*. 2014;615:390–394.
81. Sridhar V, Chun HH, Park H. 3D functional hetero-nanostructures of vertically anchored metal oxide nanowire arrays on porous graphene substrates. *Carbon*. 2014;79:330–336.
82. Lu LQ, Wang Y. Sheet-like and fusiform  $\text{CuO}$  nanostructures grown on graphene by rapid microwave heating for high Li-ion storage capacities. *J Mater Chem*. 2011;21:17916–17921.
83. Zhou XY, Zhang J, Su QM, Shi JJ, Liu Y, Du GH. Nanoleaf-on-sheet  $\text{CuO}$ /graphene composites: Microwave-assisted assemble and excellent electrochemical performances for lithium ion batteries. *Electrochim Acta*. 2014;125:615–621.
84. Hu T, Xie M, Zhong J, et al. Porous  $\text{Fe}_2\text{O}_3$  nanorods anchored on nitrogen-doped graphenes and ultrathin  $\text{Al}_2\text{O}_3$  coating by atomic layer deposition for long-lived lithium ion battery anode. *Carbon*. 2014;76:141–147.
85. Zhu XJ, Zhu YW, Murali S, Stoller MD, Ruoff RS. Nanostructured reduced graphene oxide/ $\text{Fe}_2\text{O}_3$  composite as a high-performance anode material for lithium ion batteries. *ACS Nano*. 2011;5(4):3333–3338.
86. Zhang M, Lei DN, Yin XM, et al. Magnetite/graphene composites: microwave irradiation synthesis and enhanced cycling and rate performances for lithium ion batteries. *J Mater Chem*. 2010;20:5538–5543.
87. Bhuvaneswari S, Pratheeksha PM, Anandan S, Rangappa D, Gopalan R, Rao TN. Efficient reduced graphene oxide grafted porous  $\text{Fe}_3\text{O}_4$  composite as a high performance anode material for Li-ion batteries. *Phys Chem Chem Phys*. 2014;16:5284–5294.
88. Yu SH, Conte DE, Baek S, et al. Structure-properties relationship in iron oxide-reduced graphene oxide nanostructures for Li-ion batteries. *Adv Funct Mater*. 2013;23:4293–4305.
89. Zou YQ, Kan J, Wang Y.  $\text{Fe}_2\text{O}_3$ -graphene rice-on-sheet nanocomposite for high and fast lithium ion storage. *J Phys Chem C*. 2011;115:20747–20753.
90. Li L, Guo ZP, Du AJ, Liu HK. Rapid microwave-assisted synthesis of  $\text{Mn}_3\text{O}_4$ -graphene nanocomposite and its lithium storage properties. *J Mater Chem*. 2012;22:3600–3605.
91. Noerochim L, Wang JZ, Wexler D, Chao Z, Liu HK. Rapid synthesis of free-standing  $\text{MoO}_3$ /Graphene films by the microwave hydrothermal method as cathode for bendable lithium batteries. *J Power Sources*. 2013;228:198–205.
92. Palanisamy K, Kim Y, Kim H, Kim JM, Yoon WS. Self-assembled porous  $\text{MoO}_3$ /graphene microspheres towards high performance anodes for lithium ion batteries. *J Power Sources*. 2015;275:351–361.
93. Hsieh CT, Lin CY, Chen YF, Lin JS. Synthesis of  $\text{ZnO}$ @Graphene composites as anode materials for lithium ion batteries. *Electrochim Acta*. 2013;111:359–365.
94. Li N, Song HW, Cui H, Yang GW, Wang CX. Self-assembled growth of  $\text{Sn}$ @CNTs on vertically aligned graphene for binder-free high Li-storage and excellent stability. *J Mater Chem A*. 2014;2:2526–2537.
95. Chen SQ, Wang Y, Ahn H, Wang GX. Microwave hydrothermal synthesis of high performance tin-graphene nanocomposites for lithium ion batteries. *J Power Sources*. 2012;216:22–27.
96. Beck FR, Epur R, Hong D, Manivannan A, Kumta PN. Microwave derived facile approach to  $\text{Sn}$ /Graphene composite anodes for, lithium-ion batteries. *Electrochim Acta*. 2014;127:299–306.
97. Li N, Song HW, Cui H, Wang CX.  $\text{Sn}$ @graphene grown on vertically aligned graphene for high-capacity, high-rate, and long-life lithium storage. *Nano Energy*. 2014;3:102–112.
98. Thomas R, Rao KY, Rao GM. Enhanced electrochemical performance of graphene nanosheet thin film anode decorated with tin nanoparticles. *Mater Express*. 2014;4(1):65–71.
99. Baek S, Yu SH, Park SK, et al. A one-pot microwave-assisted non-aqueous sol-gel approach to metal oxide/graphene nanocomposites for Li-ion batteries. *RSC Adv*. 2011;1:1687–1690.

100. Zhong C, Wang JZ, Chen ZX, Liu HK. SnO<sub>2</sub>-graphene composite synthesized via an ultrafast and environmentally friendly microwave autoclave method and its use as a superior anode for lithium-ion batteries. *J Phys Chem C*. 2011;15:25115–25120.
101. Lu HL, Li NW, Zheng MB, et al. Microwave-assisted synthesis of graphene-SnO<sub>2</sub> nanocomposite for rechargeable lithium-ion batteries. *Mater Lett*. 2014;115:125–128.
102. Zhu YQ, Li C, Cao CB. Strongly coupled mesoporous SnO<sub>2</sub>-graphene hybrid with enhanced electrochemical and photocatalytic activity. *RSC Adv*. 2013;3:11860–11868.
103. Chen TQ, Pan LK, Liu XJ, Yu K, Sun Z. One-step synthesis of SnO<sub>2</sub>-reduced graphene oxide-carbon nanotube composites via microwave assistance for lithium ion batteries. *RSC Adv*. 2012;2:11719–11724.
104. Liu LL, An MZ, Yang PX, Zhang JQ. Superior cycle performance and high reversible capacity of SnO<sub>2</sub>/graphene composite as an anode material for lithium-ion batteries. *Sci Rep*. 2015;5:9055.
105. Wang DN, Li XF, Wang JJ, et al. Defect-rich crystalline SnO<sub>2</sub> immobilized on graphene nanosheets with enhanced cycle performance for Li ion batteries. *J Phys Chem C*. 2012;116:22149–22156.
106. Birrozzi A, Raccichini R, Nobili F, Marinaro M, Tossici R, Marassi R. High-stability graphene nano sheets/SnO<sub>2</sub> composite anode for lithium ion batteries. *Electrochim Acta*. 2014;137:228–234.
107. Li D, Seng KH, Shi DQ, Chen ZX, Liu HK, Guo ZP. A unique sandwich-structured C/Ge/graphene nanocomposite as an anode material for high power lithium ion batteries. *J Mater Chem A*. 2013;1:14115–14121.
108. Wang CD, Chui YS, Li Y, Chen XF, Zhang WJ. Binder-free Ge-three dimensional graphene electrodes for high-rate capacity Li-ion batteries. *Appl Phys Lett*. 2013;103:253903.
109. Maroni F, Raccichini R, Birrozzi A, et al. Graphene/silicon nanocomposite anode with enhanced electrochemical stability for lithium-ion battery applications. *J Power Sources*. 2014;269:873–882.
110. Wang CD, Chui YS, Ma RG, et al. A three-dimensional graphene scaffold supported thin film silicon anode for lithium-ion batteries. *J Mater Chem A*. 2013;1:10092–10098.
111. Shanmugaraj AM, Ryu SH. Excellent electrochemical performance of graphene-silver nanoparticle hybrids prepared using a microwave spark assistance process. *Electrochim Acta*. 2012;74:207–214.
112. Hsieh CT, Lin CY, Chen YF, Lin JS, Teng H. Silver nanorods attached to graphene sheets as anode materials for lithium-ion batteries. *Carbon*. 2013;62:109–116.
113. Chen P, Su Y, Liu H, Wang Y. Interconnected tin disulfide nanosheets grown on graphene for Li-ion storage and photocatalytic applications. *ACS Appl Mater Interfaces*. 2013;5:12073–12082.
114. Gu Y, Wang Y. Microwave hydrothermal growth of In<sub>2</sub>S<sub>3</sub> interconnected nanoflowers and nanoparticles on graphene for high-performance Li-ion batteries. *RSC Adv*. 2014;4:8582–8589.
115. Shi Y, Gao J, Abruña HD, et al. Rapid synthesis of Li<sub>4</sub>Ti<sub>3</sub>O<sub>12</sub>/graphene composite with superior rate capability by a microwave-assisted hydrothermal method. *Nano Energy*. 2014;8:297–304.
116. Kim HK, Jegal JP, Kim JY, Yoon SB, Roh KC, Kim KB. In situ fabrication of lithium titanium oxide by microwave-assisted alkalization for high-rate lithium-ion batteries. *J Mater Chem A*. 2013;1:14849–14852.
117. Kim HK, Bak SM, Kim KB. Li<sub>4</sub>Ti<sub>3</sub>O<sub>12</sub>/reduced graphite oxide nanohybrid material for high rate lithium-ion batteries. *Electrochem Commun*. 2010;12:1768–1771.
118. Yan X, Li YJ, Du F, et al. Synthesis and optimizable electrochemical performance of reduced graphene oxide wrapped mesoporous TiO<sub>2</sub> microspheres. *Nanoscale*. 2014;6:4108–4116.
119. Kang WP, Tang YB, Li WY, et al. Porous CuCo<sub>2</sub>O<sub>4</sub> nanocubes wrapped by reduced graphene oxide as high-performance lithium-ion battery anodes. *Nanoscale*. 2014;6:6551–6556.
120. Zhong C, Wang JZ, Wexler D, Liu HK. Microwave autoclave synthesized multi-layer graphene/single-walled carbon nanotube composites for free-standing lithium-ion battery anodes. *Carbon*. 2014;66:637–645.
121. Chen TQ, Pan LK, Yu K, Sun Z. Microwave-assisted synthesis of reduced graphene oxide-carbon nanotube composites as negative electrode materials for lithium ion batteries. *Solid State Ionics*. 2012;229:9–13.
122. Zou F, Hu XL, Sun YM, et al. Microwave-induced in situ synthesis of Zn<sub>3</sub>GeO<sub>8</sub>/N-doped graphene nanocomposites and their lithium-storage properties. *Chem Eur J*. 2013;19:6027–6033.
123. Bae SH, Karthikeyan K, Lee YS, Oh IK. Microwave self-assembly of 3D graphene-carbon nanotube-nickel nanostructure for high capacity anode material in lithium ion battery. *Carbon*. 2013;64:527–536.
124. Lee SH, Sridhar V, Jung JH, et al. Graphene-nanotube-iron hierarchical nanostructure as lithium ion battery anode. *ACS Nano*. 2013;7(5):4242–4251.
125. Praneetha S, Murugan AV. A rapid, one-pot microwave-solvothermal synthesis of a hierarchical nanostructured graphene/LiFePO<sub>4</sub> hybrid as a high performance cathode for lithium ion batteries. *RSC Adv*. 2013;3:25403–25409.
126. Shi Y, Chou SL, Wang JZ, et al. Graphene wrapped LiFePO<sub>4</sub>/C composites as cathode materials for Li-ion batteries with enhanced rate capability. *J Mater Chem*. 2012;22:16465–16470.
127. Wang ZZ, Guo HF, Yan P. A rapid microwave heating route to synthesize graphene modified LiFePO<sub>4</sub>/C nanocomposite for rechargeable lithium-ion batteries. *Ceram Int*. 2014;40:15801–15806.
128. Roh HK, Kim HK, Roh KC, Kim KB. LiTi<sub>2</sub>(PO<sub>4</sub>)<sub>3</sub>/reduced graphene oxide nanocomposite with enhanced electrochemical performance for lithium-ion batteries. *RSC Adv*. 2014;4:31672–31677.
129. Bak SM, Nam KW, Lee CW, et al. Spinel LiMn<sub>2</sub>O<sub>4</sub>/reduced graphene oxide hybrid for high rate lithium ion batteries. *J Mater Chem*. 2011;21:17309–17315.
130. Carlo LD, Conte DE, Kemnitz E, Pinna N. Microwave-assisted fluorolytic sol-gel route to iron fluoride nanoparticles for Li-ion batteries. *Chem Commun*. 2014;50:460–462.

## Reports in Electrochemistry

### Publish your work in this journal

Reports in Electrochemistry is an international, peer-reviewed, open access journal publishing original research, reports, reviews and commentaries on all areas of electrochemistry. The manuscript management system is completely online and includes a very quick and fair peer-

review system. Visit <http://www.dovepress.com/testimonials.php> to read real quotes from published authors.

Submit your manuscript here: <http://www.dovepress.com/reports-in-electrochemistry-journal>

Dovepress